Journal of Fluids and Structures (1998) **12,** 225–258

NUMERICAL STUDY OF THE FLOW PATTERN AND THE IN-LINE RESPONSE OF A FLEXIBLE CYLINDER IN AN OSCILLATING STREAM

P. ANAGNOSTOPOULOS AND G. ILIADIS

Department of Civil Engineering, University of Thessaloniki, Thessaloniki 54006, Greece

(Received 1 July 1996 and in revised form 17 November 1997)

If an elastically mounted cylinder free to move in the streamwise direction is immersed in an oscillating stream, oscillations are very likely to be induced on the cylinder under the action of the fluctuating in-line force. In the present investigation, a numerical solution of the in-line oscillations of a circular cylinder is presented for a fixed Reynolds number equal to 200 and Keulegan–Carpenter numbers ranging between 2 and 20. The finite element method was used for the solution of the Navier–Stokes equations in the formulation where the stream function and vorticity are the field variables. For each Keulegan–Carpenter number considered, various frequency ratios were examined, the frequency ratio being defined as the ratio of the flow oscillation frequency to the natural frequency of the cylinder in air. For all frequency ratios investigated, the time histories of the cylinder response and of the hydrodynamic forces exerted on the cylinder were calculated, and the effect of the cylinder motion on the flow pattern was examined. The drag and added mass coefficients of the total in-line force exerted on the cylinder were also evaluated.

1. INTRODUCTION

Oscillatory flow past a circular cylinder provides a simplified two-dimensional idealization of the more complicated wave–body interaction. The phenomenon is controlled by two dimensionless numbers, the Reynolds number, $\mathrm{Re} = U_m D/\nu$, based on the maximum flow velocity U_m, and the Keulegan–Carpenter number, defined as $\mathrm{KC} = U_m T/D$, where T is the period of flow oscillation. The ratio of these two numbers is known as the frequency parameter, β, and is defined as $\beta = \mathrm{Re}/\mathrm{KC}$, which equals $D^2/\nu T$.

Several experimental investigations of the phenomenon have been conducted throughout a wide range of Reynolds and Keulegan–Carpenter numbers. Experiments at low KC have revealed that the flow can be classified into a number of different flow regimes governed mainly by KC and dependent also on Re (Bearman *et al.* 1981; Williamson 1985; Sarpkaya 1986; Tatsuno & Bearman 1990). For KC lower than a critical value which depends on the frequency parameter, the flow remains symmetrical. If this critical KC is exceeded, the flow becomes asymmetric and various vortex shedding flow regimes are observed, at which the number of vortices shed in each oscillation cycle increases with the Keulegan–Carpenter number. Apart from the experimental work, the increase of efficiency of digital computers allowed the numerical solution of the phenomenon. Baba & Miyata (1987), Murashige *et al.* (1989), Wang & Dalton (1991) and Justesen (1991) obtained finite difference solutions of the Navier–Stokes equations for a wide range of Keulegan–Carpenter and Reynolds numbers. Graham & Djahansouzi (1989), Skomedal *et al.* (1989) and Smith & Stansby (1991) used discrete vortex methods for the computation of two-dimensional oscillating flow past

0889-9746/98/030225 + 34 $25.00/fl970139

a cylinder. In addition, Anagnostopoulos *et al.* (1993) and Iliadis & Anagnostopoulos (1998*a*, *b*) presented finite element solutions of oscillatory flow around a circular cylinder.

The oscillating flow has as effect the generation of a large fluctuating force in the streamwise direction. This force contains components at the fundamental and higher harmonics of the incident flow, which become more significant as the Keulegan–Carpenter number increases. If the cylinder is elastically mounted, its response in the streamwise direction will be amplified when its natural frequency is close to any of these components, but principally at the fundamental frequency. Moreover, the shedding of vortices in the asymmetric regime is associated with the generation of a fluctuating force in the transverse direction, which, under certain conditions, may induce oscillations on a cylinder free to vibrate in the cross-flow direction.

The hydrodynamic excitation of elastically supported cylinders in oscillatory flow has been the subject of numerous investigations because, apart from the academic interest of the phenomenon, the response of structural members of submerged structures is of great concern to the marine industry. An approximate solution of the in-line response of a flexible cylinder based on the linearized equations of motion has been given by Blevins (1977). McConnel & Park (1982), Bearman & Hall (1987), Maull & Kaye (1988), Borthwick & Herbert (1990), Bearman & Mackwood (1991), Bearman *et al.* (1992) and Lipsett & Williamson (1994) conducted experiments on the hydrodynamic response of compliant cylinders in oscillating and wave flow. The cylinder was free to move in the streamwise direction, transversely to the incident flow, or in both directions. Graham & Djahansouzi (1991) used a discrete vortex method for the prediction of the excitation of a compliant cylinder in two directions, and Bearman *et al.* (1994) used a similar technique for the calculation of the cylinder response transversely to the oscillating stream. Anagnostopoulos *et al.* (1995) used a finite element technique for the investigation of the cylinder response in the streamwise direction, at low Keulegan–Carpenter numbers.

This paper presents numerical results of the in-line oscillations of a circular cylinder in an oscillating stream at $\mathrm{Re} = 200$ and KC ranging between 2 and 20. The finite element method was employed for the solution of the Navier–Stokes equations, in a formulation where the stream function and vorticity compose the field variables. For each Keulegan–Carpenter number considered, the solution was performed for a wide range of frequency ratios $f_r = f_f/f_n$, where f_f is the frequency of the oscillating flow and f_n is the natural frequency of the elastically mounted cylinder in air. The cylinder mass and the damping ratio were maintained constant, while the natural frequency of the cylinder was varied by adjusting the stiffness of the elastic support. Apart from the cylinder response and the hydrodynamic forces when the cylinder was oscillating, the effect of the cylinder oscillation on the flow pattern was also examined.

2. THE NUMERICAL SOLUTION

2.1. The Governing Equations and the Computational Technique

The mathematical model of the problem consists of the Navier–Stokes equations, in the formulation where the stream function Ψ and the vorticity ζ are the field variables. If n and $n + 1$ are two successive time levels separated by a time interval Δt, the governing equations become

$$\nabla^2 \Psi_n = -\zeta_n, \tag{1}$$

$$\frac{\partial \zeta_n}{\partial t} + \frac{\partial \Psi_n}{\partial y}\frac{\partial \zeta_n}{\partial x} - \frac{\partial \Psi_n}{\partial x}\frac{\partial \zeta_n}{\partial y} = \nu \nabla^2 \zeta_{n+1}. \tag{2}$$

The finite element method was used for the numerical solution of these equations. Applying Galerkin's method to equations (1) and (2) for each element and assembling for the whole continuum, as explained by Smith & Brebbia (1975, 1977) and Anagnostopoulos (1989), we obtain

$$[K_1]\{\Psi\}_n = [K_2]\{\zeta\}_n + \{R_1\}, \tag{3}$$

$$[K_3]\{\zeta\}_{n+1} + [K_4]\{\dot{\zeta}\}_n + \{R_2\} = \{R_3\}, \tag{4}$$

where $\dot{\zeta}$ represents the derivative of ζ with respect to time. The coefficient matrices $[K_1]$, $[K_2]$, $[K_3]$ and $[K_4]$ are square, whereas $\{R_1\}$, $\{R_2\}$ and $\{R_3\}$ are column matrices. The matrices $\{R_1\}$ and $\{R_3\}$ contain the derivatives of Ψ and ζ with respect to the direction n normal to the boundary, as shown in Figure 1, when the corresponding element lies on a boundary and a natural boundary condition for Ψ or ζ is specified.

Expressing $\dot{\zeta}$ as

$$\dot{\zeta}_n = \frac{\zeta_{n+1} - \zeta_n}{\Delta t},$$

equation (4) becomes

$$\left[[K_3] + \frac{1}{\Delta t}[K_4]\right]\{\zeta\}_{n+1} = \frac{1}{\Delta t}[K_4]\{\zeta\}_n - \{R_2\}, \tag{5}$$

since the natural boundary condition for ζ is $\partial\zeta/\partial n = 0$, rendering the matrix $\{R_3\}$ equal to zero.

2.2. The Boudary Conditions for Ψ and ζ

The time-dependent free stream velocity $U(t)$ of the oscillatory flow is defined as

$$U(t) = U_m \sin(2\pi t/T), \tag{6}$$

where U_m is the maximum flow velocity and T is the period of the flow oscillation.

At the inflow and outflow boundaries, the stream function varies linearly according to the relationship

$$\Psi = U(t)y, \tag{7}$$

where y is the distance of the point considered from the horizontal axis of symmetry of the solution domain. The stream function on the lateral boundaries is constant and can be determined from equation (7).

The values of the stream function on the cylinder surface are derived from the impermeability condition, namely

$$\frac{\partial \Psi}{\partial s} = U_c \cos\theta, \tag{8}$$

where U_c is the instantaneous cylinder velocity and s the tangential direction, as illustrated in Figure 1.

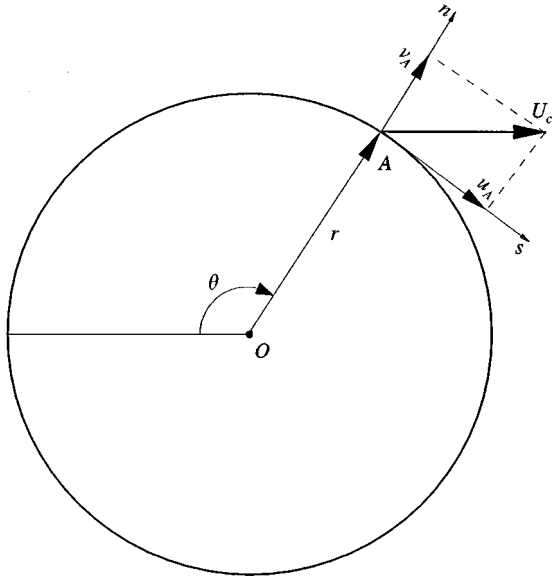

Figure 1. Definition sketch.

The vorticity was assumed equal to zero throughout the outer boundaries, while along a no-slip boundary it can be calculated from the formula

$$\zeta_1 = \frac{3\int_S (u\,\mathrm{d}x + v\,\mathrm{d}y)}{\Delta} - (\zeta_2 + \zeta_3), \tag{9}$$

which is easily derived from the relationship between the vorticity and circulation over an element; ζ_1 is the vorticity at node 1 lying on the solid boundary, and ζ_2 and ζ_3 the vorticity values at the two other nodes of the element. The two components of the fluid velocity are denoted as u and v, while Δ is the area of the element considered. The integration domain S is around the whole perimeter of the element. The integration in equation (9) was conducted interpolating linearly u and v from the nodal values of velocities.

2.3. Calculations of Shear, Pressure and Forces

The pressure distribution throughout the flow field can be calculated from the solution of Poisson's equation

$$\frac{\partial^2 p}{\partial x^2} + \frac{\partial^2 p}{\partial y^2} = -2\rho\left(\frac{\partial u}{\partial y}\frac{\partial v}{\partial x} - \frac{\partial u}{\partial x}\frac{\partial v}{\partial y}\right). \tag{10}$$

The application of Galerkin's method to equation (10) for an element, and assembly throughout the domain, yields

$$[K_5][p] = [R_4] + [R_5], \tag{11}$$

in which the element r_{5i} of the column matrix $\{R_5\}$ is given from

$$r_{5i} = \int_S \frac{\partial p}{\partial n}\,\mathrm{d}s. \tag{12}$$

The integration is performed at the part of the boundary where a natural boundary condition for pressure is specified. In the present case, natural boundary conditions for pressure are specified on the cylinder surface and on the inflow and outflow boundaries.

The momentum equation for a fluid element in the radial direction on the cylinder surface yields the boundary condition for pressure on the cylinder as

$$\frac{\partial p}{\partial n} = \mu \frac{\partial \zeta}{\partial s} + \rho A_c \cos\theta, \tag{13}$$

where A_c is the instantaneous cylinder acceleration, derived from the solution of equation (19) in which it is denoted as $\ddot{x}$. On the other hand, the momentum equation in the streamwise direction on the inflow and outflow boundaries of the computational domain where the vorticity is zero yields

$$\frac{\partial p}{\partial n} = -\rho \frac{\mathrm{d}U}{\mathrm{d}t}, \tag{14}$$

where U is the instantaneous stream velocity given by equation (6). Substituting $\partial p/\partial n$ from equations (13) and (14) in equation (12) the matrix $\{R_5\}$ can be evaluated.

The shear stress on the cylinder was calculated from the vorticity ζ_w at the boundary as

$$\tau_w = 2\mu \frac{U_c}{r} \sin\theta - \mu\, \zeta_w, \tag{15}$$

where μ denotes the viscosity of the fluid.

The in-line and transverse forces per unit cylinder length are calculated from the integration of shear and pressure around the cylinder as

$$F_x^* = \int_0^{2\pi} p \cos\theta \,\mathrm{d}\theta + \int_0^{2\pi} \tau_w \sin\theta \,\mathrm{d}\theta, \tag{16}$$

$$F_y^* = -\int_0^{2\pi} p \sin\theta \,\mathrm{d}\theta + \int_0^{2\pi} \tau_w \cos\theta \,\mathrm{d}\theta, \tag{17}$$

where θ is the angle defining the location of the point considered from the leading edge of the cylinder in the clockwise direction. F_x^* and F_y^* can be nondimensionlized according to the formulae

$$F_x = \frac{F_x^*}{\frac{1}{2}\rho U_m^2 D} \quad \text{and} \quad F_y = \frac{F_y^*}{\frac{1}{2}\rho U_m^2 D}. \tag{18}$$

2.4. The Computational Mesh and the Solution Algorithm

The generation of a suitable grid network is very important, since the accuracy and economy of the solution depend greatly on the form of the computational mesh. The criteria imposed by Iliadis & Anagnostopoulos (1998*a*) for the generation of a grid suitable for the solution of oscillatory flow around a fixed cylinder were also applied to the oscillating cylinder case. The computational grid contains three-node triangular elements, as shown in the sample of Figure 2. In the part of the solution domain near the cylinder where a refined grid was used, the nodal points were placed on circles concentric to the cylinder

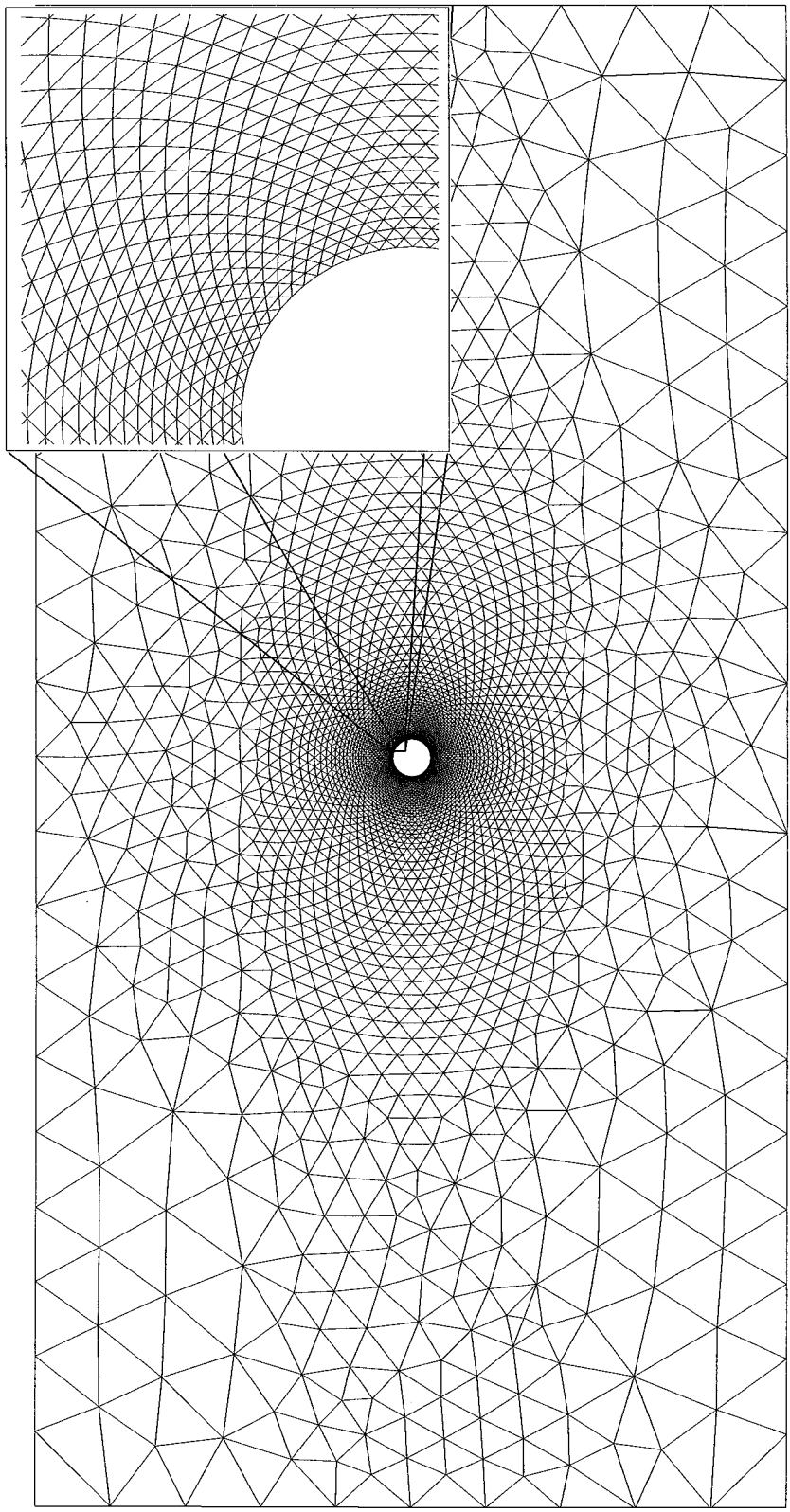

Figure 2. The finite element mesh, containing 3352 nodes and 6580 elements.

cross-section. The element size in the vicinity of the cylinder was very small, increasing gradually with the distance from the cylinder, as shown in the enlarged view near the cylinder appearing in the window. An important issue is the element size close to the cylinder compared to the boundary layer thickness δ of the oscillating flow. As explained by Iliadis & Anagnostopoulos (1998*a*), the boundary layer thickness δ can be approximated from the formula $\delta/D \approx 4/(2\pi\beta)^{1/2}$, which was derived from the velocity distribution around an oscillating flat plate. The highest value of β considered herein was 100, yielding the minimum δ equal to $0{\cdot}16D$. Thus, the finite element mesh of Figure 2 is adequate for the resolution of flow within the boundary layer for $\beta = 100$. The same computational grid was employed for the solution at lower values of β, although the increasing values of the boundary layer thickness would permit the use of a coarser mesh near the cylinder.

The inflow and outflow boundaries of the mesh depicted in Figure 2 had been located 20 cylinder diameters upstream and downstream from the cylinder centre. This mesh was used for the study of the vortex shedding cases, in which the vortices shed are convected far from the cylinder. In the case of symmetrical flow where the vortices remain attached to the cylinder, these boundaries were placed 10 cylinder diameters upstream and downstream from the cylinder, in order to reduce the computational time required.

In the present study, the cylinder motion was restricted in the streamwise direction, therefore, the cylinder was performing oscillations under the action of the fluctuating in-line force. The equation of motion of an elastically supported cylinder excited by a time-dependent force $F(t)$ is

$$m\ddot{x} + c\dot{x} + kx = F(t), \tag{19}$$

where m is the cylinder mass, c the damping coefficient and k the spring stiffness. The cylinder displacement, velocity and acceleration are denoted as x, $\dot{x}$ and $\ddot{x}$, respectively. In our case the exciting force $F(t)$ is the in-line force F_x^* calculated from equation (16) at time t. For the solution of equation (19) and the derivation of the parameters of cylinder motion, a fourth-order accurate Runge–Kutta scheme was employed.

One of the difficulties encountered in the solution of flow–body interaction problems is that the position of the cylinder is not constant, but varies continually within the solution domain. Various solutions exist of the cross-flow oscillations of a compliant cylinder in a uniform stream using an Eulerian description of the Navier–Stokes equations in the stream-function–vorticity formulation (Anagnostopoulos 1989, 1994) or Lagrangian–Eulerian schemes of the N-S equations expressed in primitive variables (Mittal & Tezduyar 1992; Nomura & Hughes 1992; Nomura 1993; Wei *et al.* 1995). In the Eulerian description, the computational grid was translated with the cylinder at each time step, and the nodal values of vorticity calculated from equation (5) were interpolated linearly to new grid locations.

Thus, the solution algorithm consists of the following steps:

(a) evaluation of the stream function at time t (level n) from equation (3); the nodal values of vorticity, except those lying on the solid boundary, are those calculated in the previous iteration at the displaced grid locations as explained previously, or, in particular, the initial conditions;

(b) the vorticity values at the no-slip boundary are updated from equation (9);

(c) the vorticity at time $t + \Delta t$ (level $n + 1$) is calculated from equation (5);

(d) the hydrodynamic forces are evaluated from equations (16) and (17);

(e) the parameters of the cylinder motion at time $t + \Delta t$ are derived from equation (19).

3. COMPUTATIONAL RESULTS

Computations were performed at Re = 200 and KC equal to 2, 4, 10 and 20. In all cases the solution started assuming zero vorticity throughout the solution domain. The cylinder was released from the position of zero deflection and started to move under the action of the in-line force. For each KC considered, the cylinder response was examined for a wide range of frequency ratios $f_r = f_f/f_n$, where f_f is the frequency of the oscillating stream and $f_n = \omega_n/2\pi = (k/m)^{1/2}/2\pi$ the natural frequency of the cylinder in air. The mass of the cylinder m was assumed equal to 0·01 kg per unit length, while the damping ratio $\zeta = c/2m\omega_n$ was held constant, and equal to 0·05 throughout the procedure. The frequency ratio may be written as

$$f_r = \frac{f_f}{f_n} = \frac{1/T_f}{\sqrt{k/m}/2\pi} = \frac{2\pi}{T_f\sqrt{k/m}}, \tag{20}$$

which yields

$$k = \frac{4\pi^2 m}{T_f^2 f_r^2}. \tag{21}$$

Equation (21) indicates that for constant m and f_r, the higher values of flow period T_f prevailing at increased values of KC yield lower values of k. High values of f_r have also the same effect when m and T_f are maintained constant. Considering that $c = 2\zeta\sqrt{km}$, it is evident that, as the values of KC or f_r are increased, both k and c decrease. These lower values of k and c may lead to amplified cylinder response for higher values of KC and f_r.

For Re = 200, depending on KC, the flow pattern around a fixed cylinder can be characterized as: (a) symmetrical with respect to the wake centre-line; (b) asymmetric, in which the flow is periodic and vortex shedding occurs; and (c) aperiodic, where the vortex shedding pattern is different at consecutive cycles. This classification of flow pattern will be used for the presentation of the results.

3.1. The Symmetrical Flow

For KC equal to 2 and 4 the flow remains symmetrical with respect to the wake centre-line. The time history of the cylinder displacement was similar for both KC values, but the amplitude at steady state was greater for KC = 4. The time history of the cylinder displacement for various frequency ratios f_r at KC = 4 is presented in Figure 3. The oscillation amplitude builds up gradually and is stabilized after a number of oscillation cycles which depends on the frequency ratio. When $f_r \neq 1$, the total motion of the cylinder is a superposition of the decaying free motion of the cylinder at its natural frequency and the forced motion due to the oscillating in-line force. After a few periods from the beginning of the oscillation, the transient disappears and the amplitude is stabilized at a value which depends on the frequency ratio. It is evident that, apart from the case $f_r = 1$ where resonant conditions occur, the amplitude of oscillation is very small.

The time histories of the in-line force, cylinder displacement and stream velocity over two oscillation cycles at constant amplitude for frequency ratios 0·3 and 1 are depicted in Figures 4 and 5. For frequency ratio equal to 0·3 the cylinder displacement diverges from the pure harmonic motion and the phase angle between the exciting force and cylinder displacement is very small, which is not the case for frequency ratio equal to 1.

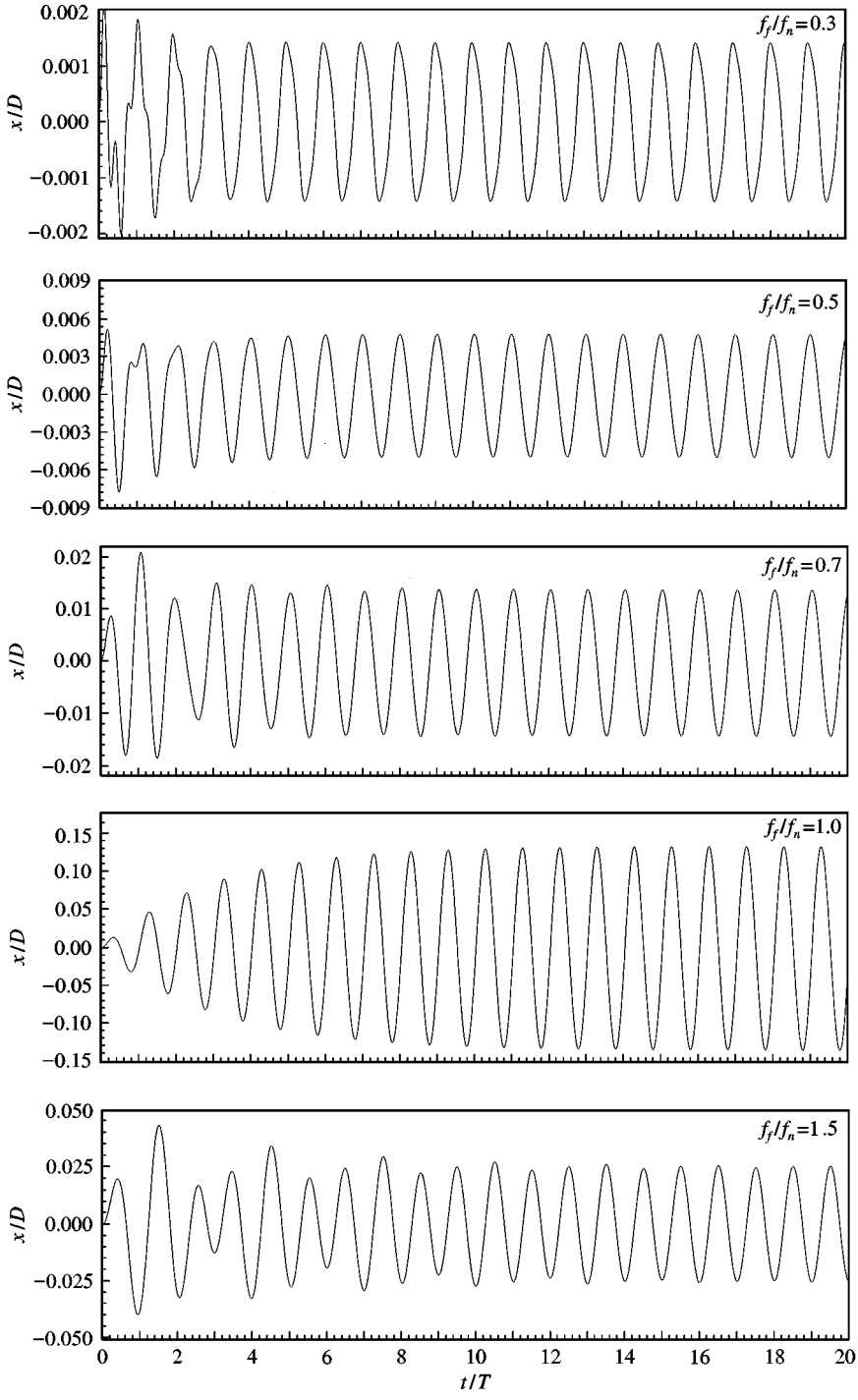

Figure 3. Time history of the cylinder displacement for various frequency ratios; KC = 4.

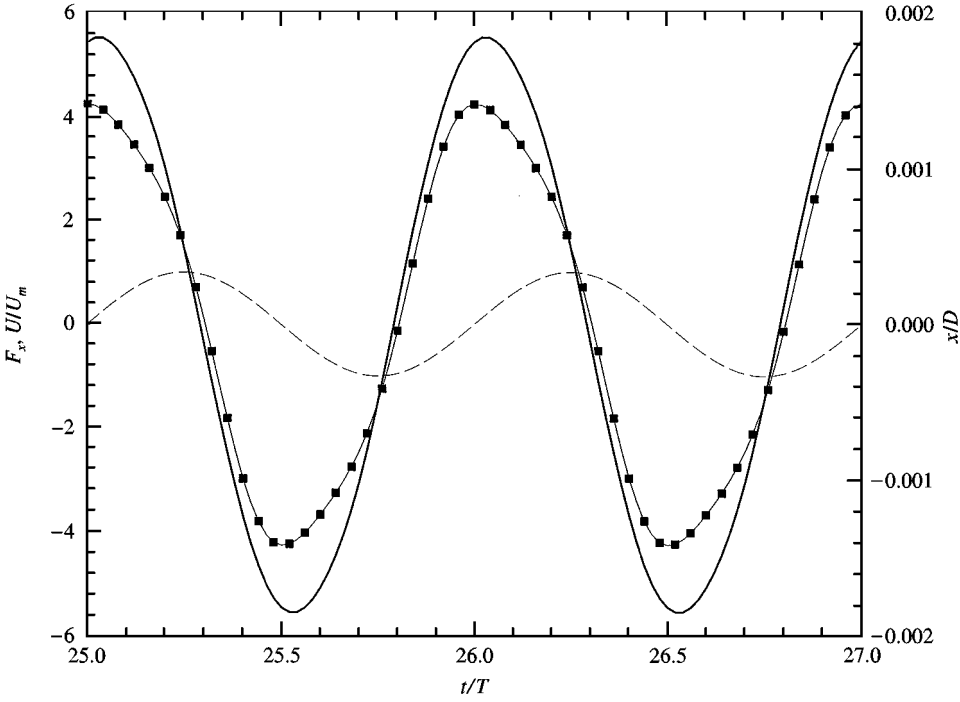

Figure 4. Traces of cylinder displacement, in-line force and stream velocity for KC = 4; and $f_f/f_n = 0{\cdot}3$. –■–, x/D; —, F_x; – – –, U/U_m.

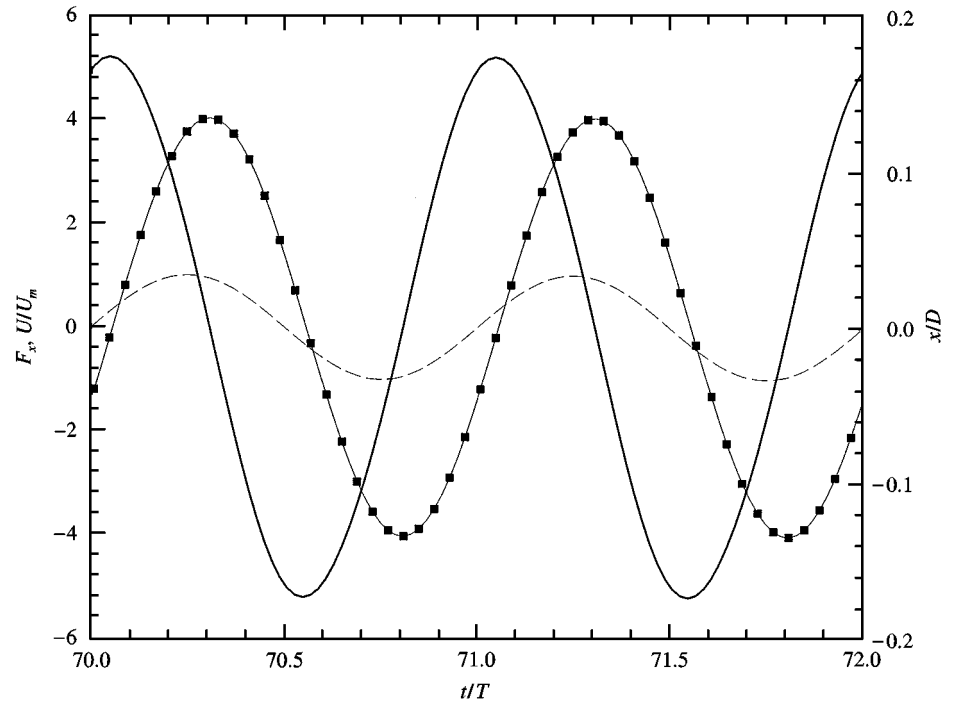

Figure 5. Traces of cylinder displacement, in-line force and stream velocity for KC = 4; and $f_f/f_n = 1$. –■–, x/D; –, F_x; – – –, U/U_m.

The oscillation amplitude and phase angle at steady state as functions of the frequency ratio for KC = 4 are depicted in Figure 6. For frequency ratio equal to 1, the phase angle is slightly higher than 90°. When the oscillation frequency is lower than the natural frequency, the phase angle is lower than 90°, whereas when the frequency of oscillation exceeds the cylinder natural frequency the phase angle is higher than 90°.

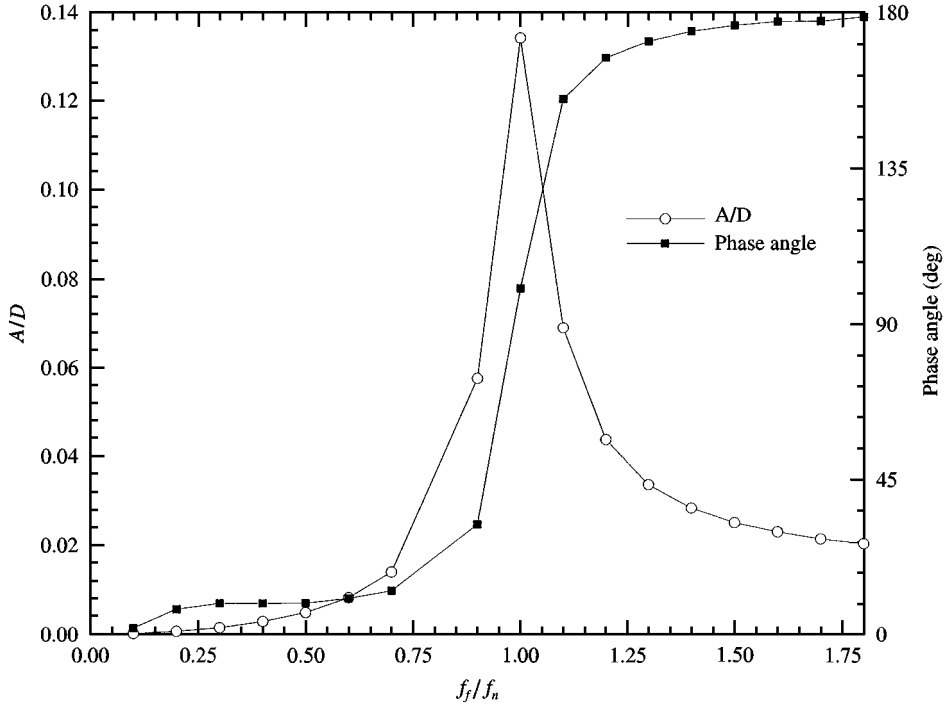

Figure 6. Oscillation amplitude and phase angle at steady state as functions of the frequency ratio, for KC = 4; the cylinder mass was 0·01 kg, and the damping ratio 0·05.

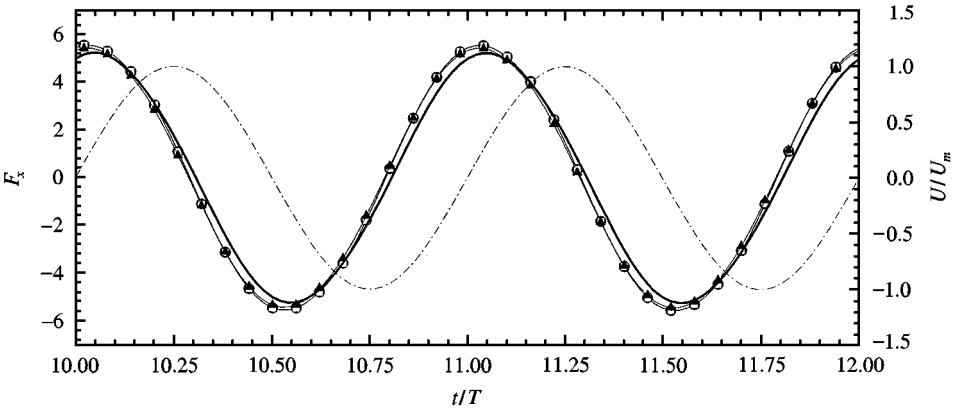

Figure 7. Time history of the in-line force exerted on the cylinder for various frequency ratios; KC = 4. –●–, $f_f/f_n = 0{\cdot}1$; –□–, $f_f/f_n = 0{\cdot}3$; —, $f_f/f_n = 1{\cdot}0$; –▲–, $f_f/f_n = 1{\cdot}5$; –·–·–, U/U_m.

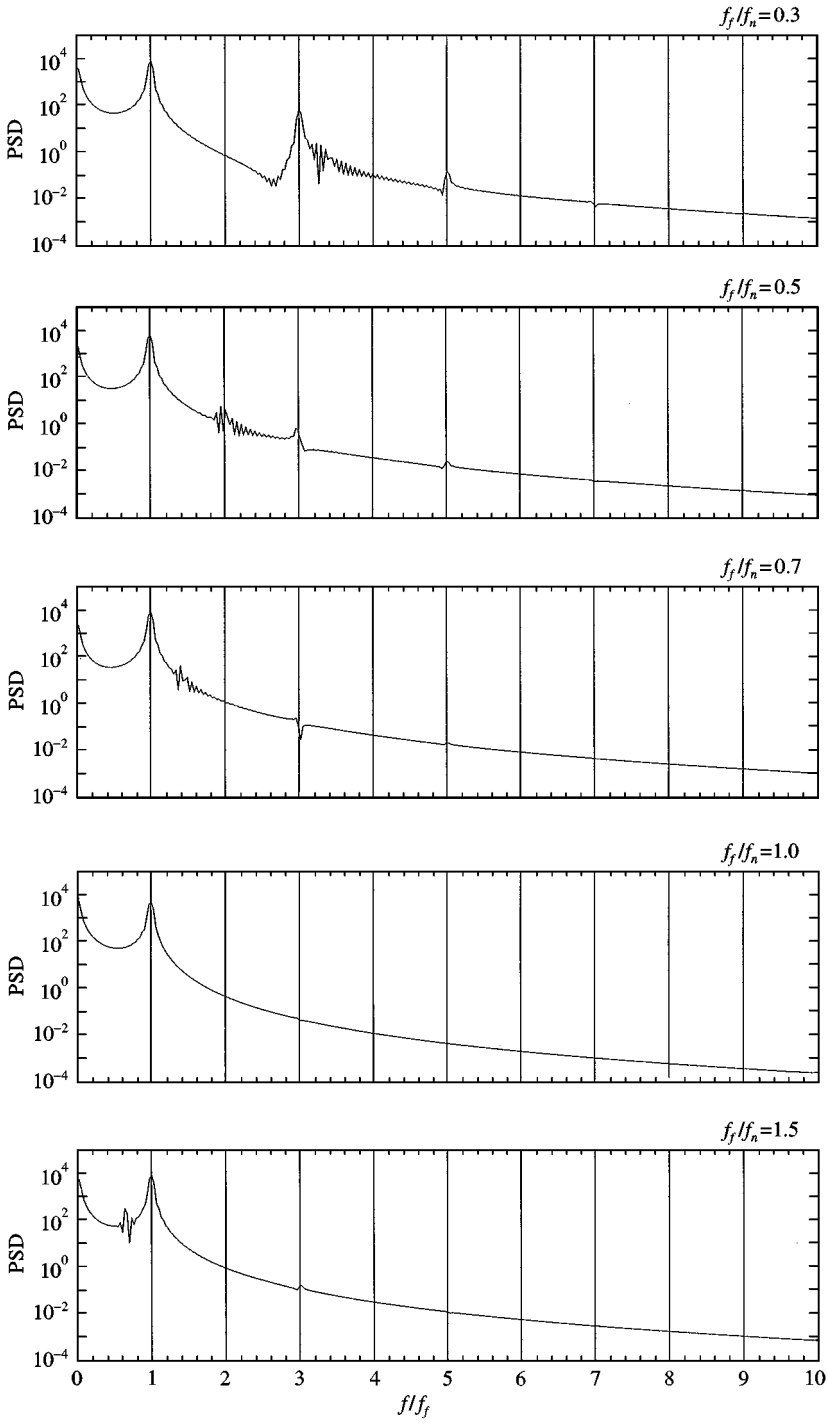

Figure 8. Power spectra of the cylinder displacement at steady state for various frequency ratios; KC = 4.

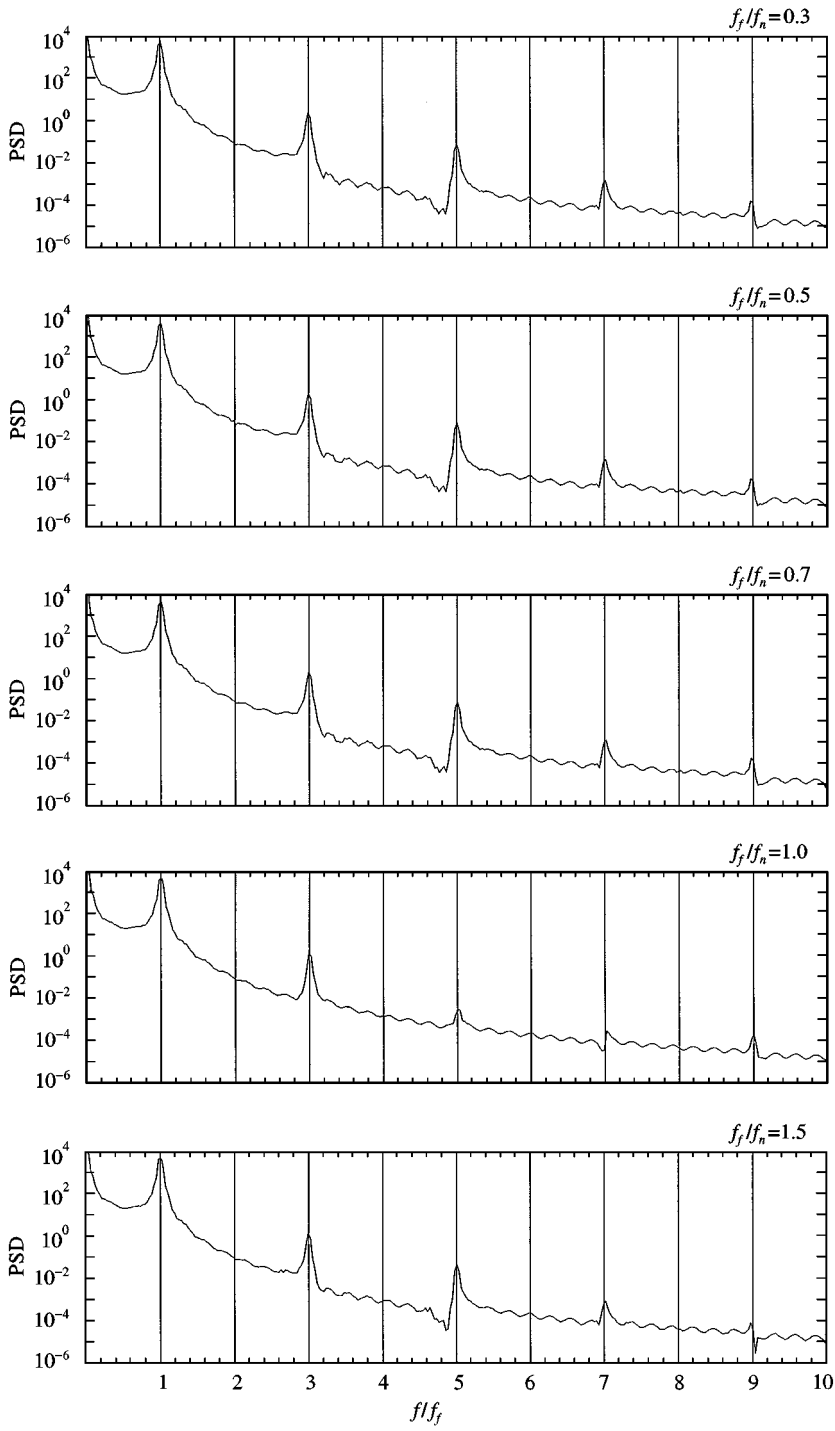

Figure 9. Power spectra of the in-line force at steady state for various frequency ratios; KC = 4.

The traces of the in-line force over two oscillation cycles for various frequency ratios are presented in Figure 7. This figure reveals that at resonance the cylinder motion has as result a slightly different force trace from those at other frequency ratios. The amplitude of the in-line force is slightly lower at resonance, and the phase angle between the force and the stream velocity has been altered.

The power spectra of the cylinder displacement when the amplitude was stabilized are presented for various frequency ratios in Figure 8, while those of the exciting force are shown in Figure 9. Figure 9 indicates that the exciting force, apart from the fundamental, contains also components at odd multiples of the flow frequency. The component at three times the flow frequency when $f_r = 0{\cdot}3$ is very close to the cylinder natural frequency and causes the peak at the same harmonic which appears in Figure 8 at the same frequency ratio. This effect is also evident in the cylinder displacement trace of Figure 4, which diverges from a sine wave.

The streamlines and equivorticity lines for $KC = 4$ over one-half of an oscillation cycle are depicted in Figure 10 for $f_r = 0{\cdot}1$ and in Figure 11 for $f_r = 1$. The solid lines correspond to positive vorticity and the dashed to negative. Throughout the study, the cross-hairs mark the position of the cylinder centre at zero deflection. In Figure 10, due to the small oscillation amplitude, the flow pattern is similar to that for a fixed cylinder, as illustrated by Iliadis & Anagnostopoulos (1998*a*). Comparison of Figures 10 and 11 reveals the effect of the cylinder motion on the flow field. The higher oscillation amplitude at $f_r = 1$ is linked to an increased size of the separation bubble formed behind the cylinder compared to the flow at $f_r = 0{\cdot}1$ for the same phase angle. An increased rate of cancellation of the vorticity upstream from the cylinder, generated during the previous half-cycle, is also apparent when $f_r = 1$.

3.2. The Asymmetric Flow

It is well known that for oscillating flow past a fixed cylinder, as the Keulegan–Carpenter number is increased over a certain value which depends also on the frequency parameter, asymmetries appear in the flow which are eventually amplified and lead finally to complex vortex shedding patterns. The visual study by Tatsuno & Bearman (1990) and the computations by Iliadis & Anagnostopoulos (1998*a*) revealed that for $KC = 10$ and $\beta = 20$ the flow pattern is characterized as "double pair", which means that a pair of vortices is shed per half-cycle of the flow oscillation. The phenomenon is fully periodic, and the direction in which each vortex pair is convected away from the cylinder remains constant.

The time history of the cylinder displacement for frequency ratios extending from 0·1 to 5 at $KC = 10$ is presented in Figure 12. Comparison with Figure 3 reveals that the oscillation amplitude at steady state is higher than that for $KC = 4$ at the same frequency ratio. As explained previously, the higher flow period at $KC = 10$ yields lower values of the spring stiffness and of the damping coefficient, which are both sources of increased amplitude. An interesting result is that for frequency ratios equal to 0·3 and 0·33, the trace of the cylinder displacement contains harmonics at three times the frequency of oscillating flow, superimposed on the flow oscillation frequency f_f. This is in agreement with the experimental study by Bearman *et al.* (1992) at a higher value of the frequency parameter, equal to 750. It is also interesting to note that the very small increase of the frequency ratio from 0·3 to 0·33 results in an increase of the oscillation amplitude by 30%.

Although the oscillation amplitude reached steady state at the 20th period when the frequency ratio was equal to 1, the hydrodynamic forces, especially the transverse, had not

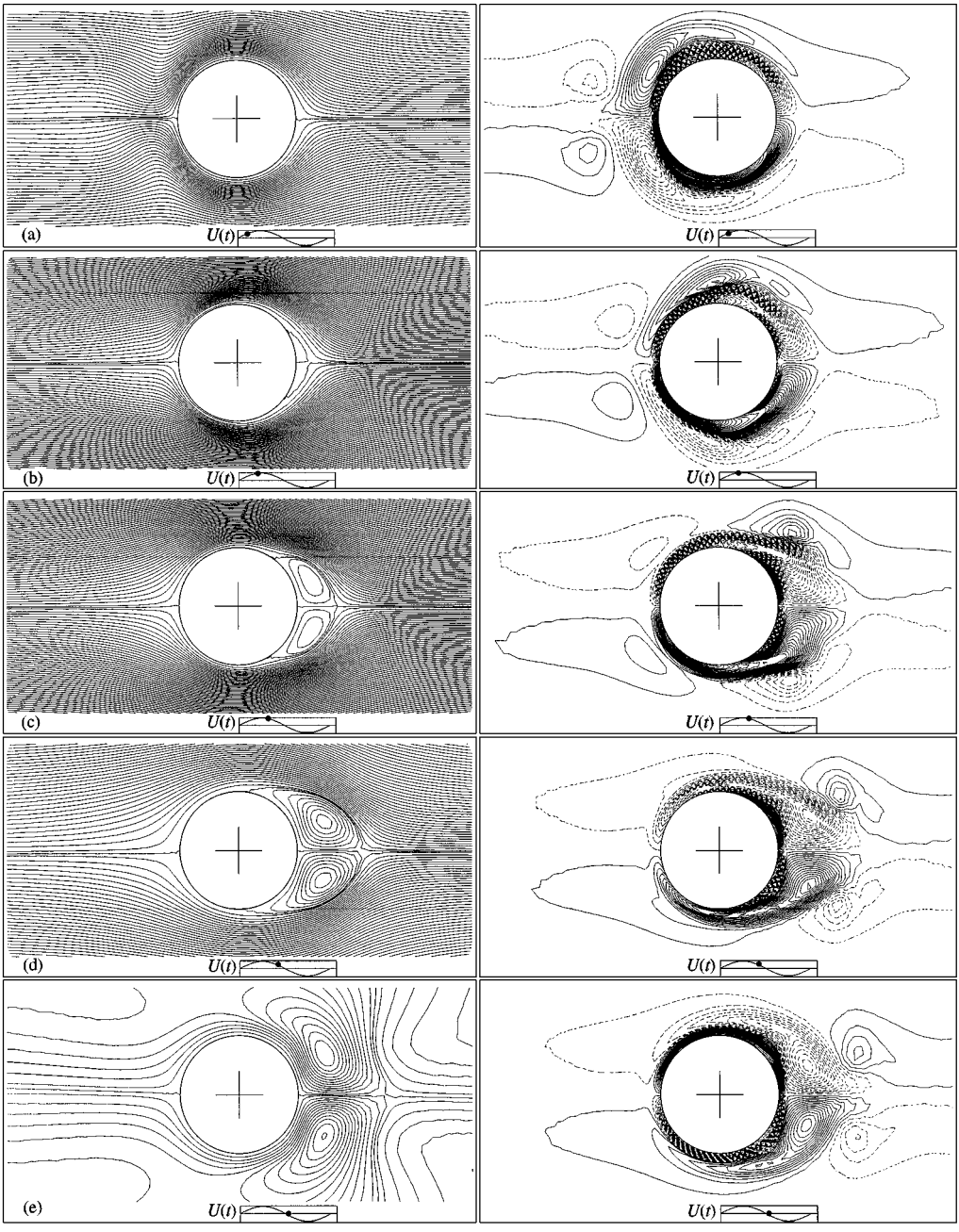

Figure 10. (I) Streamlines and (II) equivorticity lines over one-half of a period for $f_f/f_n = 0{\cdot}1$ and KC = 4. The solid lines correspond to positive vorticity and the dashed to negative. The cross-hairs mark the undeflected position of the cylinder.

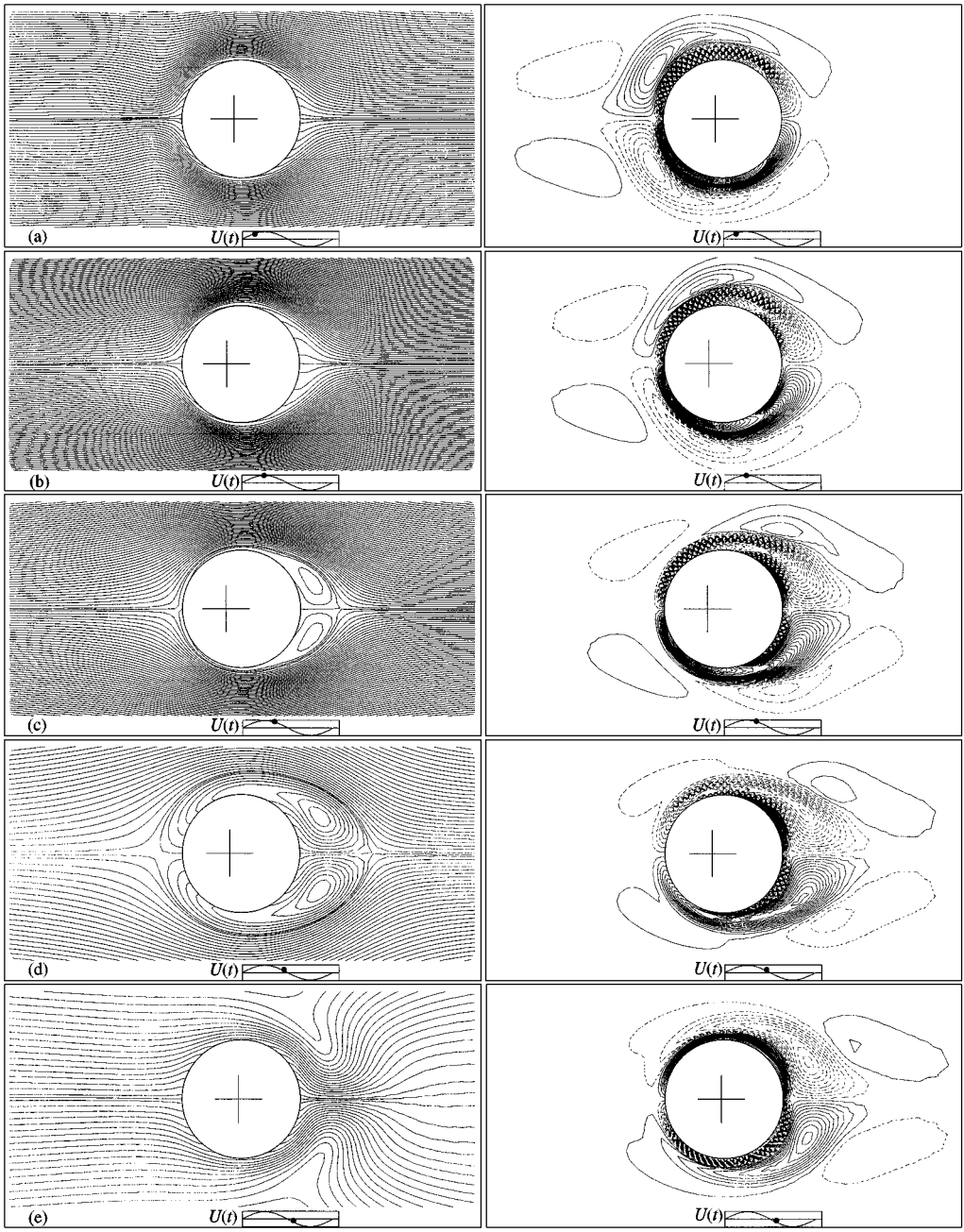

Figure 11. (I) Streamlines and (II) equivorticity lines over one-half of a period for $f_f/f_n = 1$ and KC = 4. The cross-hairs mark the undefleted position of the cylinder.

become fully periodic. The computation was continued, until the periodicity of the hydrodynamic forces and of the flow pattern was established. Traces of the hydrodynamic forces throughout the computation are shown in Figure 13. It is interesting to note that the transverse force becomes periodic after 80 oscillation cycles.

The time history of the total in-line force over two oscillation cycles for various frequency ratios is depicted in Figure 14(a), while that of the transverse force in Figure 14(b). For

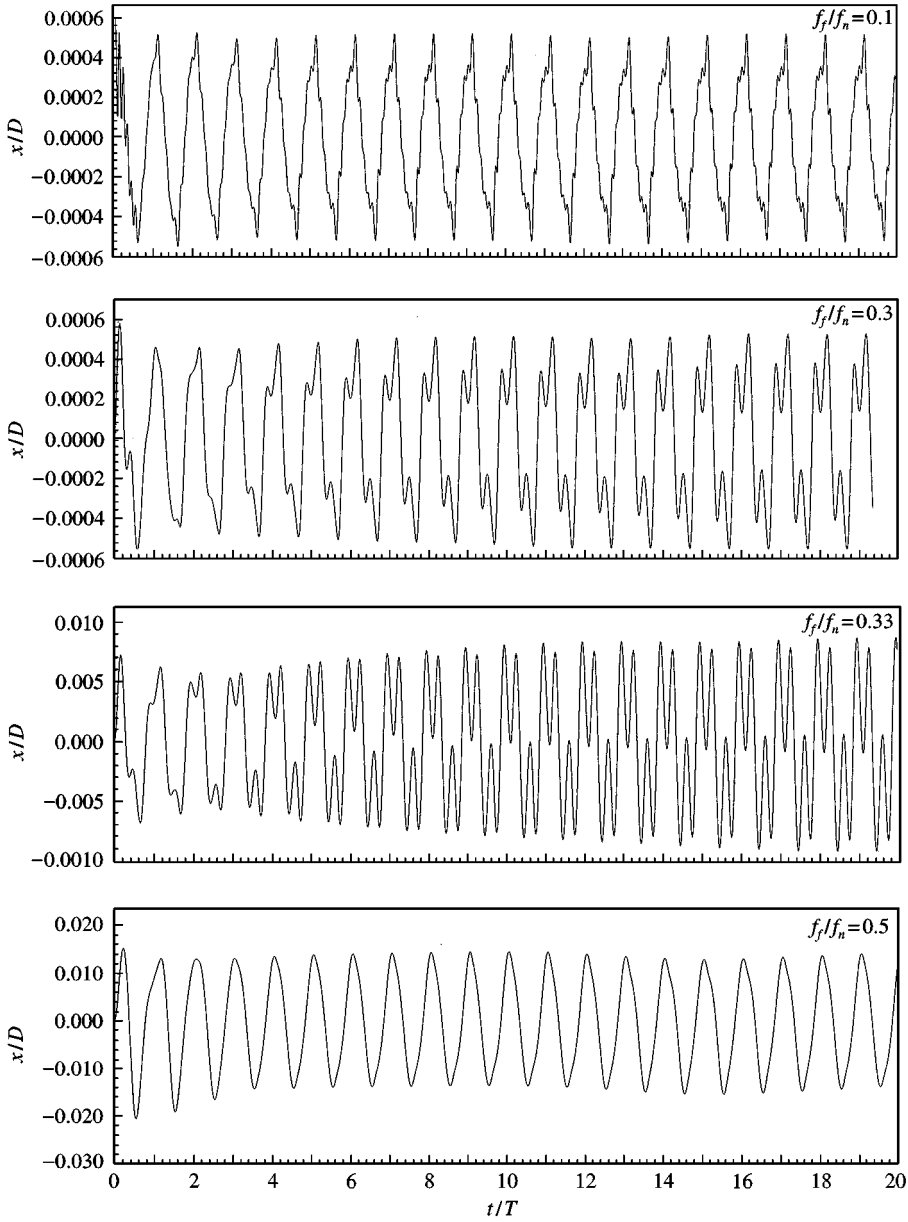

Figure 12. (a) Time history of the cylinder displacement for frequency ratios $f_f/f_n = 0{\cdot}1$ to $0{\cdot}5$; KC = 10.

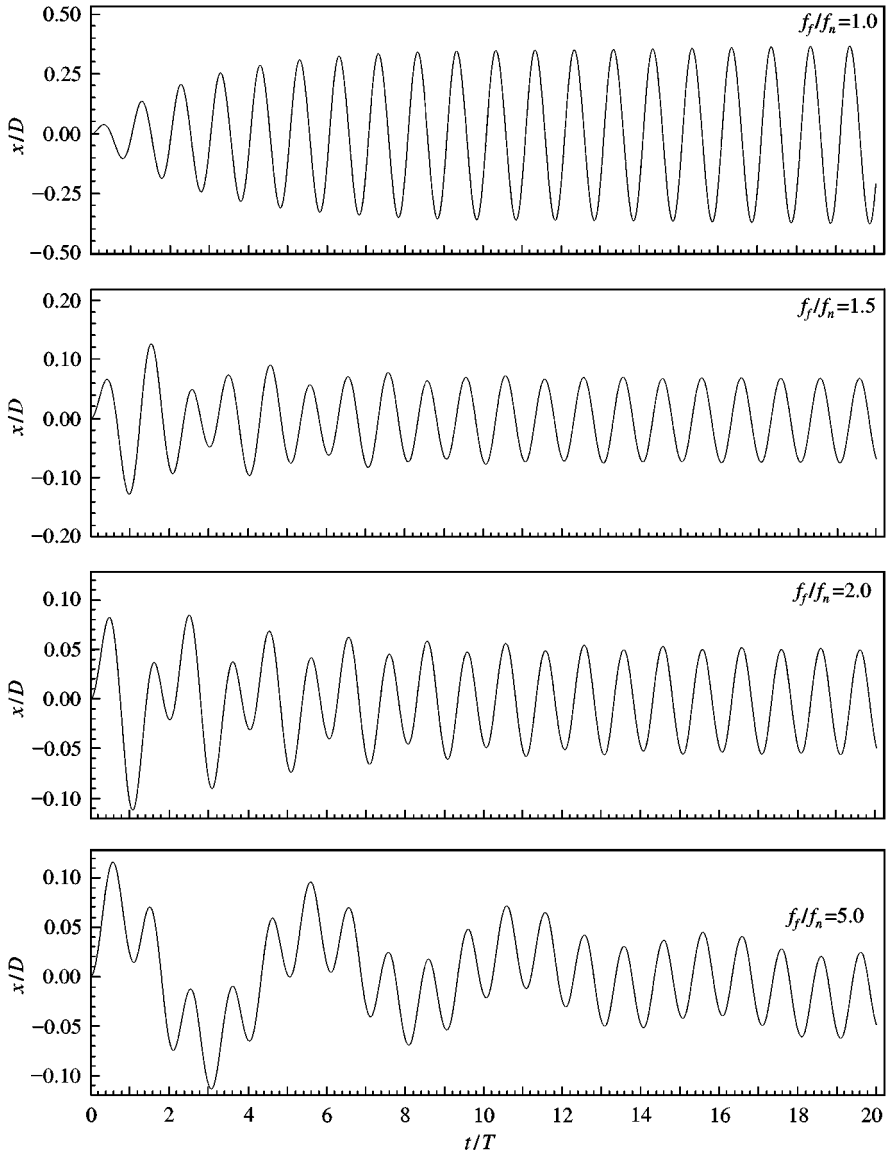

Figure 12. (b) Time history of the cylinder displacement for $f_f/f_n = 1$ to 5; KC = 10.

$f_r = 1$, the traces shown correspond to the last two periods of Figure 13, whereas for $f_r \neq 1$ to the last two periods of Figure 12. For frequency ratios different from 1, the time history of the in-line force is almost independent of the frequency ratio. For $f_r = 1$, the cylinder motion affects the in-line force trace, such that the maximum values are lower than those at other frequency ratios. Figure 14(b) indicates that the higher oscillation amplitude at $f_r = 2$ results in a lower amplitude of the transverse force than the cases where $f_r < 1$. Figure 14(b) also reveals that, at resonance, the time history of the transverse force is quite different from those observed at other frequency ratios. It is well-known from previous studies that the

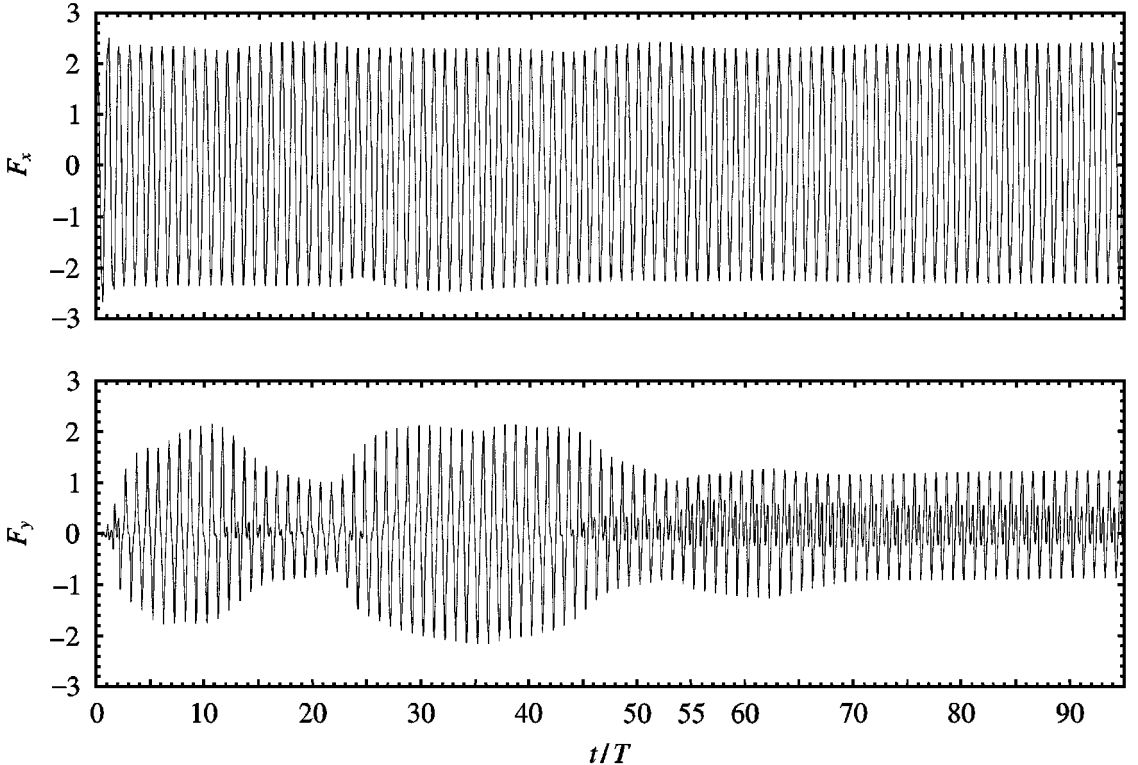

Figure 13. Time history of the hydrodynamic forces exerted on the cylinder for $f_f/f_n = 1$ and KC = 10.

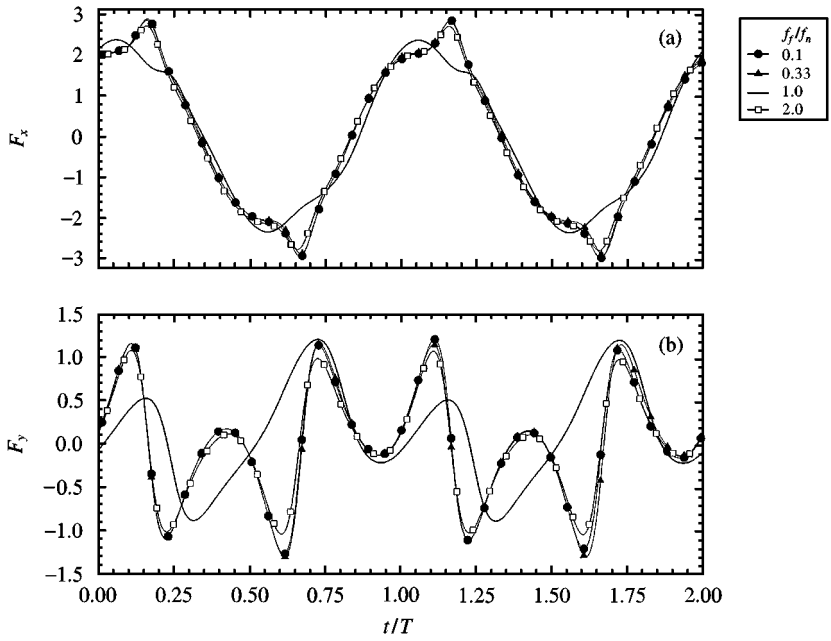

Figure 14. Time history of the hydrodynamic forces exerted on the cylinder for various frequency ratios; KC = 10.

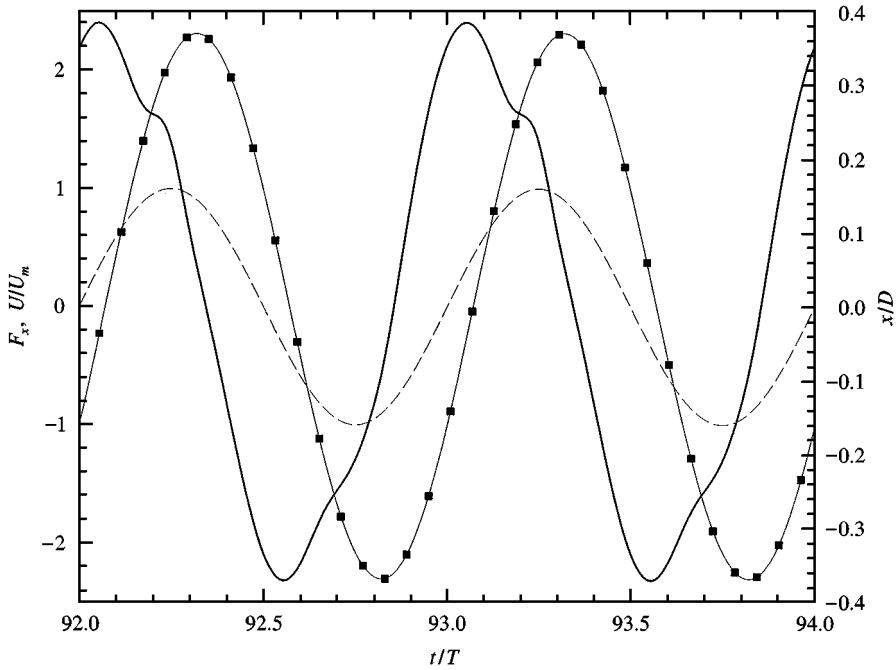

Figure 15. Traces of cylinder displacement, in-line force and stream velocity for KC = 10 and $f_f/f_n = 1$. –■–, x/D; —, F_x; – – –, U/U_m.

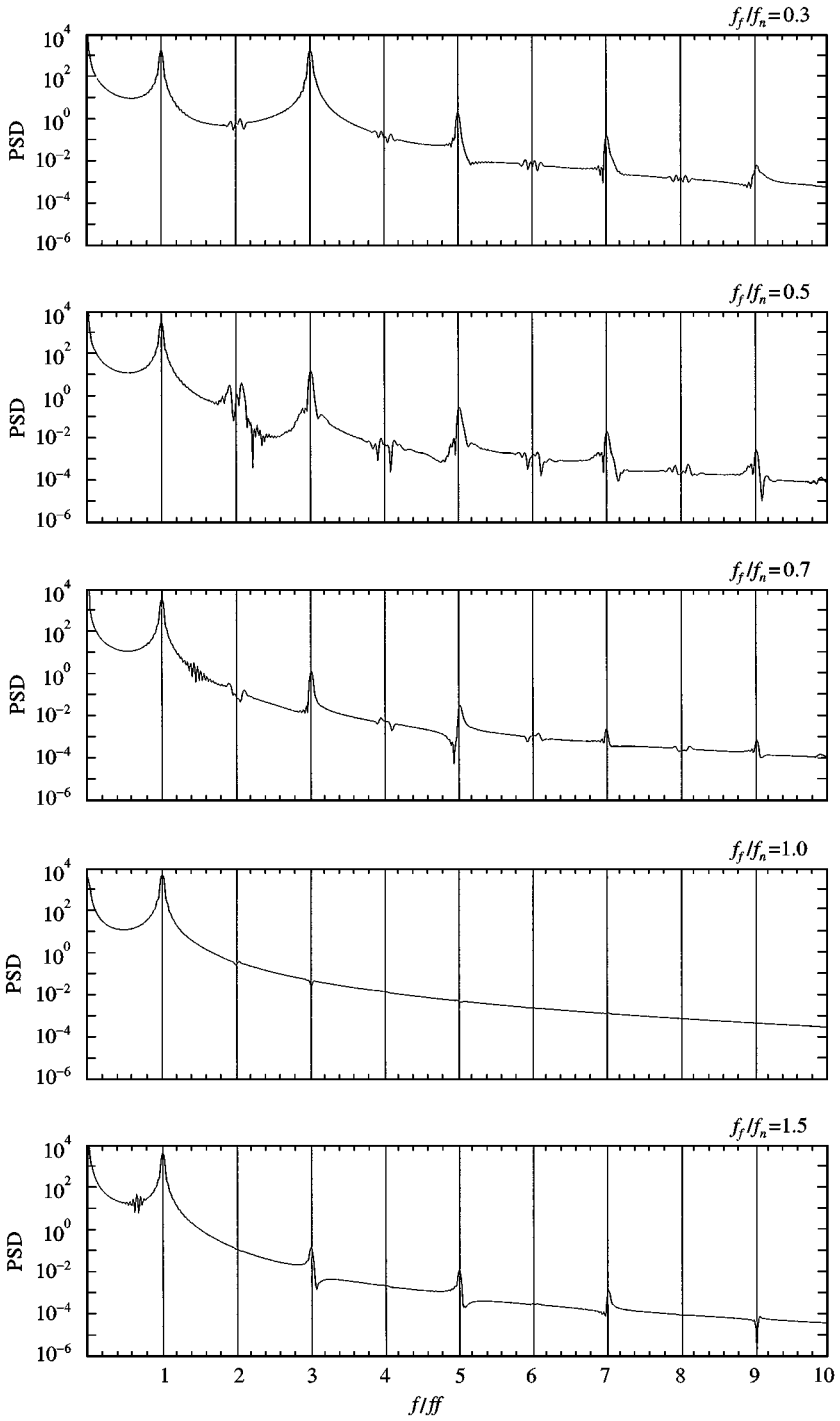

Figure 16. Power spectra of the cylinder displacement at steady state for various frequency ratios; KC = 10.

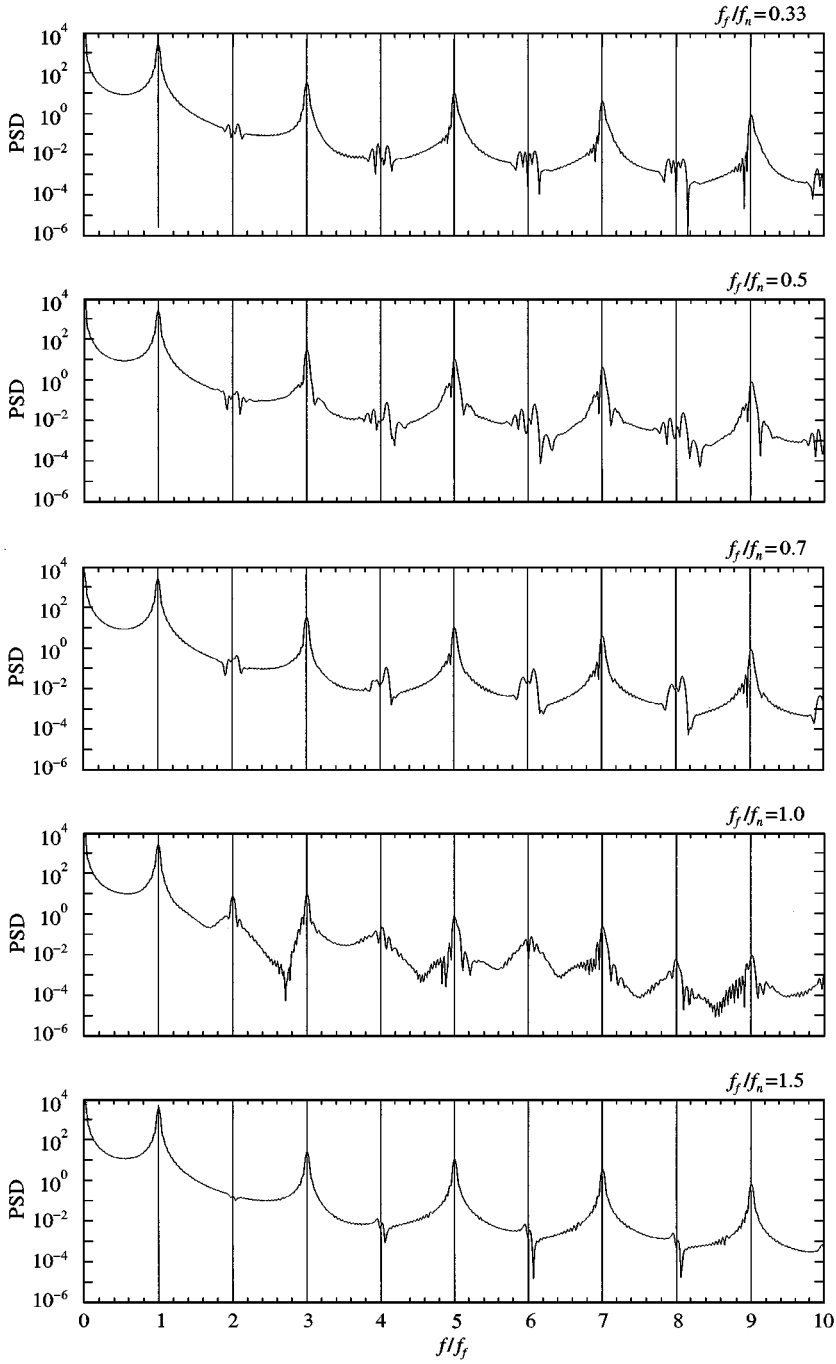

Figure 17. Power spectra of the in-line force at steady state for various frequency ratios; KC = 10.

force traces are strongly dependent on the form of the flow pattern, therefore their change at $f_r = 1$ hints at a significant alteration of the flow pattern. For all frequency ratios different from 1, the traces of the hydrodynamic forces correspond to the "double pair" for flow past a fixed cylinder, according to the computational study by Iliadis & Anagnostopoulos (1998*a*). For $f_r = 1$, the time history of the hydrodynamic forces is similar to that occurring for "oblique vortex rows" when the flow oscillates around a fixed cylinder, as found by the same authors. The traces of the stream velocity, the in-line force and the cylinder response for a frequency ratio equal to 1 are depicted in Figure 15. In spite of the fact that the force trace diverges from pure harmonic, the cylinder response is very close to a pure sine wave.

The power spectra of the cylinder displacement when the amplitude has stabilized are presented for various frequency ratios in Figure 16, while those of the exciting force in Figure 17. The component of the in-line force at the first odd multiple of the flow frequency coincides with the natural frequency of the cylinder when $f_r = 0{\cdot}33$. This component is the reason for the trace of the cylinder response in Figure 12 when $f_r = 0{\cdot}33$, where the cylinder motion at its natural frequency is superimposed on that at the flow oscillation frequency. This is verified by the power spectrum of the cylinder displacement for $f_r = 0{\cdot}33$.

It was mentioned previously that the change of the traces of the hydrodynamic forces at frequency ratio equal to 1 suggests that a significant alteration of the flow pattern has occurred. For the investigation of the effect of cylinder motion on the flow field the equi-vorticity lines were plotted for phase angle equal to 93° for a wide range of frequency ratios in Figure 18. This figure reveals that the flow pattern is that of a double pair throughout, except for frequency ratio equal to 1, where a different flow pattern appears. In frame 18(a), for example, the pairs A′–B′ and A–B were shed during the previous cycle, whereas the pair C–D is being shed from the cylinder during the present half-cycle. The nonharmonic character of the cylinder response at a frequency ratio of 0·33 has little effect on the flow pattern. For frequency ratios higher than 1, where the oscillation amplitude is greater, the vortex pairs formed at previous cycles are closer to the cylinder than in the cases where the frequency ratio is lower than 1.

The equivorticity lines over one oscillation cycle for $f_r = 1$ are presented in Figure 19. In frames 19(a–c), the flow pattern is asymmetric with respect to the wake centre-line, the vortices above the wake axis being stronger than those below. In frame 19(d), the negative sign vortex forming at the upper part of the cylinder appears in elongated form with respect to that below the cylinder, and its edge farthest from the cylinder is displaced downwards. As the flow reverses, all vortices return at the end of the cycle to the positions they occupied at the beginning of the cycle, which is the case depicted in frame 19(a). The flow pattern close to the cylinder is similar to that defined as "oblique vortex rows" by Iliadis & Anagnostopoulos (1998*a*) for oscillating flow past a fixed cylinder, a result compatible to the force traces of Figure 14. The similarity does not persist far from the cylinder, where vortex pairs are visible, instead of the parallel rows of opposite sign vortices inclined to the wake axis, upstream and downstream from the cylinder.

The oscillating stream velocity U, the cylinder velocity U_c and the relative velocity with respect to the moving cylinder $U_{\mathrm{rel}} = U - U_c$ for frequency ratio equal to 1 are depicted in Figure 20 over one oscillation cycle. The Reynolds number calculated from the maximum relative velocity is 185 and the Keulegan–Carpenter number is 9·24, while the frequency parameter remains equal to 10. When the cylinder oscillates at the steady-state amplitude, the flow is equivalent to that for a fixed cylinder immersed in an oscillating stream of velocity U_{rel}. Tatsuno & Bearman's (1990) flow visualization revealed that for $\beta = 10$ and $\mathrm{KC} = 10$ the flow pattern is a double pair, whereas a small reduction of KC at constant

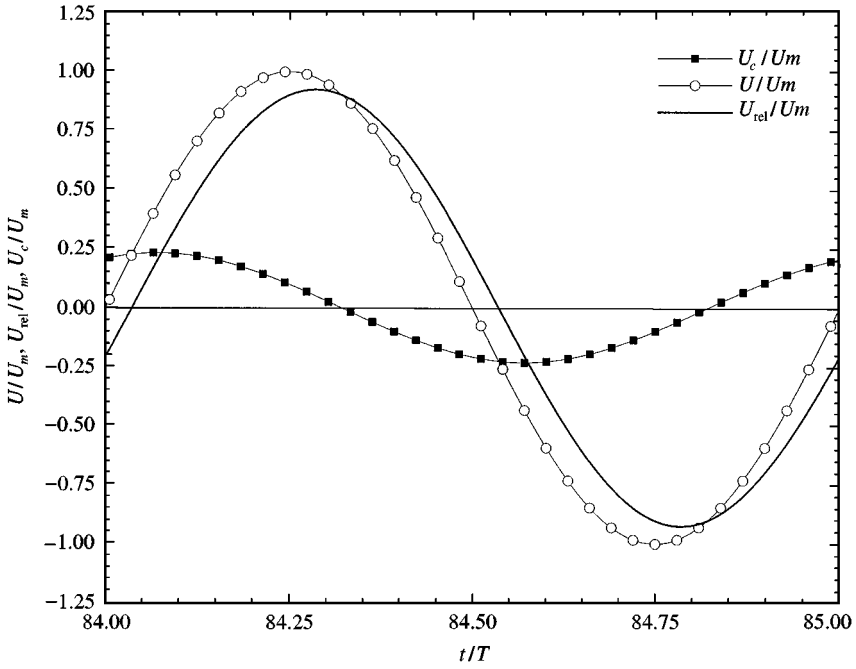

Figure 20. Stream velocity, cylinder velocity and relative velocity of flow with respect to the moving cylinder over one oscillation cycle for $f_f/f_n = 1$ and KC = 10. –■–, U_c/U_m; –○–, U/U_m; — U_{rel}/U_m.

β alters the flow to the oblique vortex rows case. The case where KC = 9·24 and $\beta = 10$ lies on the boundary between these two distinct flow regimes; therefore, characteristics of both are present. From the previous discussion it is evident that the alteration of the flow pattern when the cylinder oscillates at high amplitude is in agreement with experimental evidence within the low KC and β ranges examined in the present study.

3.3. The Aperiodic Flow

There exists an extensive regime on the KC $-$ β plane within the ranges of KC and β examined, over which the flow is aperiodic. The solution of oscillating flow around a fixed cylinder over a large number of consecutive cycles revealed that the flow switches between different modes at various oscillation cycles. It has been found by Iliadis & Anagnostopoulos (1998*b*) that for KC = 20 and $\beta = 10$ the flow is aperiodic, the only regular flow pattern observed at various cycles being the three-pair, which means that three pairs of vortices are formed per oscillation cycle.

The time history of the cylinder displacement for various frequency ratios at KC = 20 is presented in Figure 21. The oscillation amplitude at steady state is higher than that for KC = 4 and KC = 10 for the same frequency ratio. For frequency ratios equal to 0·33 and 0·35, the time history of the displacement is similar to that predicted for KC = 10, containing harmonics at three times the flow oscillation frequency, in addition to the fundamental.

To investigate the effect of cylinder oscillation on the flow pattern, the equivorticity lines were plotted at various frequency ratios. For $f_r \neq 1$, the flow was aperiodic, as in the fixed

cylinder case. The equivorticity lines over one cycle for $f_r = 0{\cdot}33$ when the amplitude was stabilized are depicted in Figure 22. Vortices C and D existing from the previous cycle, as shown in frame 22(a), pair up with the newly formed vortices A and B, which is the situation depicted in frame 22(c), and the two pairs are swept downstream by the end of the half-cycle, as illustrated in frame 22(d). As the flow reverses, vortices A′ and B′ which remained close to the cylinder after the shedding of vortices A and B, form a pair as shown in frame 22(e) and are convected towards the flow direction, whereas vortices A, B, C and D return close to the cylinder, which is the case depicted in frame 22(f). In the two following frames, vortex A finds its way behind the cylinder, vortex D remains in contact with the cylinder, whereas vortex B splits in two parts, denoted as B_1 and B_2. Vortex B_1 is convected below the cylinder, while vortex B_2 remains above and is amalgamated with the newly formed vortex G. From vortices A to D appearing in frame 22(c), A and C are almost annihilated during the rest of the cycle, and vortices B and D lose much of their initial strength. The sequence of

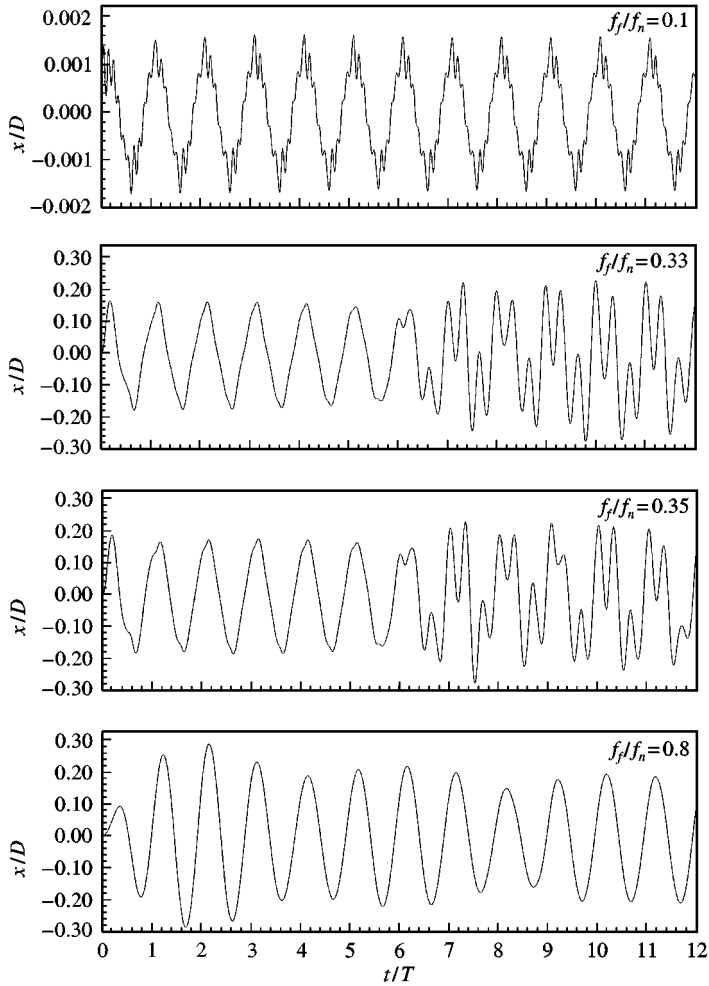

Figure 21. Time history of the cylinder displacement for various frequency ratios; KC = 20.

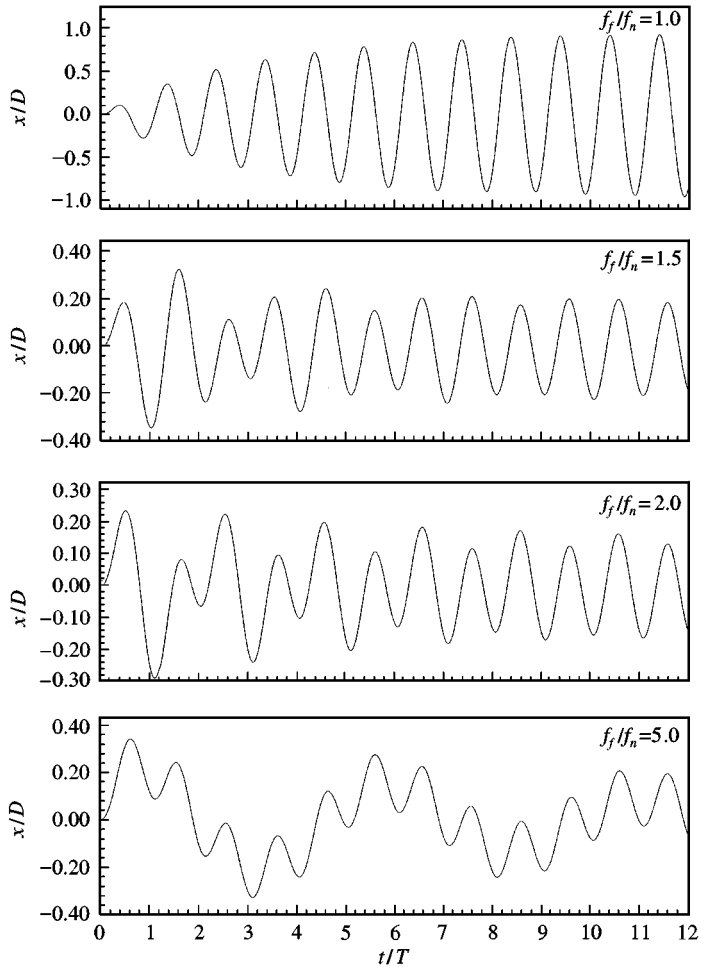

Figure 21. (*Continued*).

Figure 22 is very close to the three-pair configuration derived experimentally by Williamson (1985) and numerically by Iliadis & Anagnostopoulos (1998*b*).

The time history of the hydrodynamic forces acting on the cylinder for $f_r = 0{\cdot}33$ as the amplitude builds up is presented in Figure 23. The hydrodynamic forces after the sixth cycle become aperiodic, providing evidence of the nonperiodicity of the flow pattern. The random character of the in-line force is linked to the fluctuation of the oscillation amplitude towards the end of the time history shown in Figure 23. An interesting result is the magnification of the transverse force with time, which becomes more pronounced in the aperiodic regime.

The solution for a frequency ratio equal to 1 revealed a periodic flow pattern, quite different from that observed for other frequency ratios. The flow pattern for $f_r = 1$ over one cycle in the form of vorticity contours is depicted in Figure 24. From the sequence of frames throughout the cycle, it is evident that the flow pattern is a single pair, similar to that observed by Williamson (1985) and Justesen (1991) for KC between 12 and 15 at higher values of β. During each cycle vortices A and B_1, which comprises the greatest part of vortex

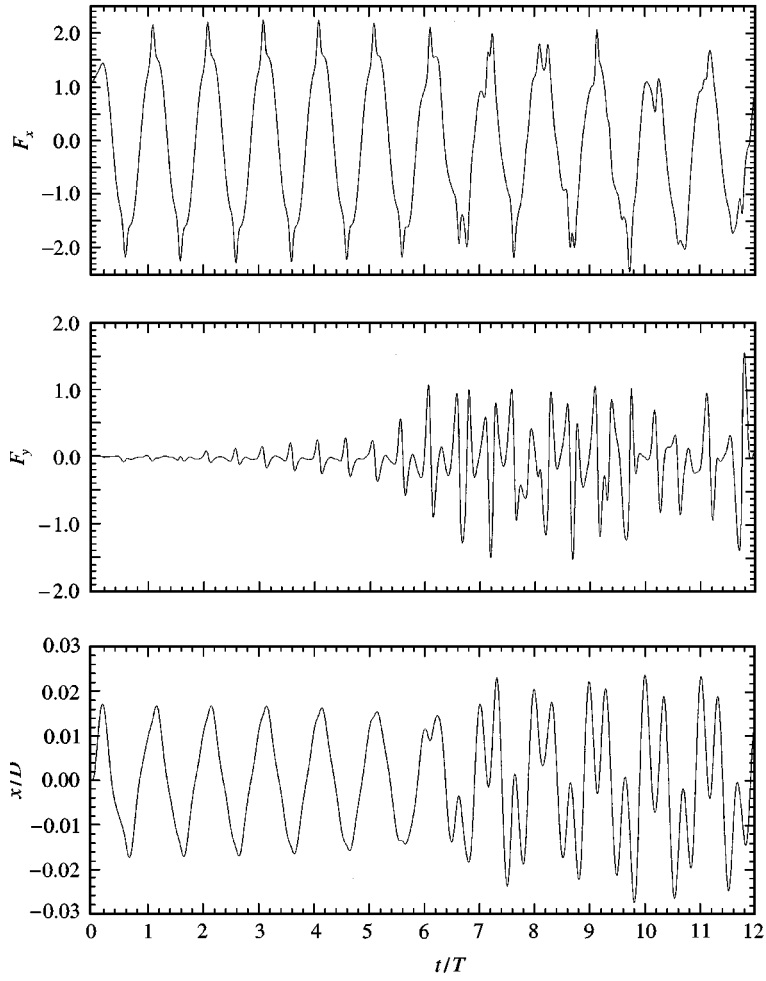

Figure 23. Traces of the hydrodynamic forces exerted on the cylinder and of the cylinder response for $f_f/f_n = 0{\cdot}33$ and KC = 20.

B, move diagonally below the cylinder, while vortices C and D are forming. The Reynolds number corresponding to the maximum relative velocity with respect to the moving cylinder is 155 and the Keulegan–Carpenter number 15.5. Thus, the reduction of the effective KC from 20, when the cylinder is kept fixed, to 15.5, when the cylinder oscillates at constant $\beta = 10$, has a drastic effect on the flow.

The traces of the hydrodynamic forces exerted on the cylinder over many oscillation cycles for frequency ratio equal to 1 are depicted in Figure 25. After a transient state, which lasts approximately 45 periods, the hydrodynamic forces become fully periodic. Of great interest is the amplification of the amplitude of the transverse force at t/T greater than 4, which becomes finally greater than that of the in-line force, as concluded from their superposition in Figure 26 over one period.

It should be stressed that the three-pair pattern occurred even for frequency ratios higher than 1, as obtained from the numerical experiments. In spite of the relatively large

oscillation amplitudes, the flow is similar to the case depicted in Figure 22 and does not exhibit the single-pair pattern which occurs at $f_r = 1$.

3.4. The Cylinder Response and the Hydrodynamic Force Coefficients

The amplitude of the cylinder oscillation at steady state for all cases considered is depicted in Figure 27. For constant frequency ratio the oscillation amplitude increases with increasing KC. It was explained in the previous context that the increase of the Keulegan–Carpenter number implies lower values of the spring stiffness and of the damping ratio, which is a source of greater cylinder response, even for a constant value of the exciting force. The oscillation amplitudes are relatively high for frequency ratios greater than 1, as expected from equation (21). Of interest is the local peak at f_r around 0·33 for KC equal to 10 and 20. For this regime of frequency ratios the exciting force contains components close to the cylinder natural frequency, which act to amplify the response.

Morison *et al.* (1950) proposed that the total-line force per unit length of a fixed cylinder of diameter D in an oscillating flow can be expressed as the sum of two components

$$F_x^* = \tfrac{1}{2}\rho D C_D U|U| + \tfrac{1}{4}\pi\rho D^2 C_M \dot{U}, \tag{22}$$

where ρ is the fluid density and C_D and C_M the drag and inertia coefficients. In the case of an elastically mounted cylinder vibrating in an oscillating fluid, Morison's equation can be written as

$$F_x^* = \tfrac{1}{2}\rho D C_D(U - \dot{x})|U - \dot{x}| + \rho A\dot{U} + C_I\rho A(\dot{U} - \ddot{x}), \tag{23}$$

where A is the cylinder cross-section, $\dot{x}$ and $\ddot{x}$ denote the velocity and acceleration of the cylinder and C_D and C_I the drag and added mass coefficients. The first term of equation (23) constitutes the drag component of the in-line force, while the inertia component consists of two parts. The first part is the buoyancy term, and the second the added mass term.

For the determination of the coefficients C_D and C_M of equation (22), Isaacson *et al.* (1991) used and compared eight different techniques. One of these techniques is the least squares fit proposed by Borgman (1972), according to which the force coefficients are estimated by minimizing the square of the difference between the time series of the computed and predicted forces. The estimated force coefficients are given from

$$C_D = \frac{2}{\rho D}\left[\frac{s_3 s_4 - s_2 s_5}{s_1 s_4 - s_2^2}\right], \quad C_M = \frac{4}{\rho\pi D^2}\left[\frac{s_2 s_3 - s_1 s_5}{s_2^2 - s_1 s_4}\right], \tag{24, 25}$$

where

$$s_1 = \sum_{i=1}^{N} U^4(i), \quad s_2 = \sum_{i=1}^{N} U(i)|U(i)|\dot{U}(i), \quad s_3 = \sum_{i=1}^{N} U(i)|U(i)|F_x^*(i),$$
$$s_4 = \sum_{i=1}^{N} \dot{U}^2(i), \quad s_5 = \sum_{i=1}^{N} \dot{U}(i)F_x^*(i). \tag{26}$$

The fluid velocity $U(i)$, acceleration $\dot{U}(i)$ and force $F_x^*(i)$ are considered at time $t = i\Delta t$; N is the total number of samples and Δt is the interval between successive time levels of the discretized records.

Equations (24)–(26) can also be used to determine the coefficients C_D and C_I in equation (23) in the case of the oscillating cylinder. The difference from the fixed cylinder case is that the relative velocity $U - \dot{x}$ and acceleration $\dot{U} - \ddot{x}$ should be used, instead of U and $\dot{U}$, for the determination of the coefficients s_1 to s_5. Moreover, since C_I is sought instead of C_M,

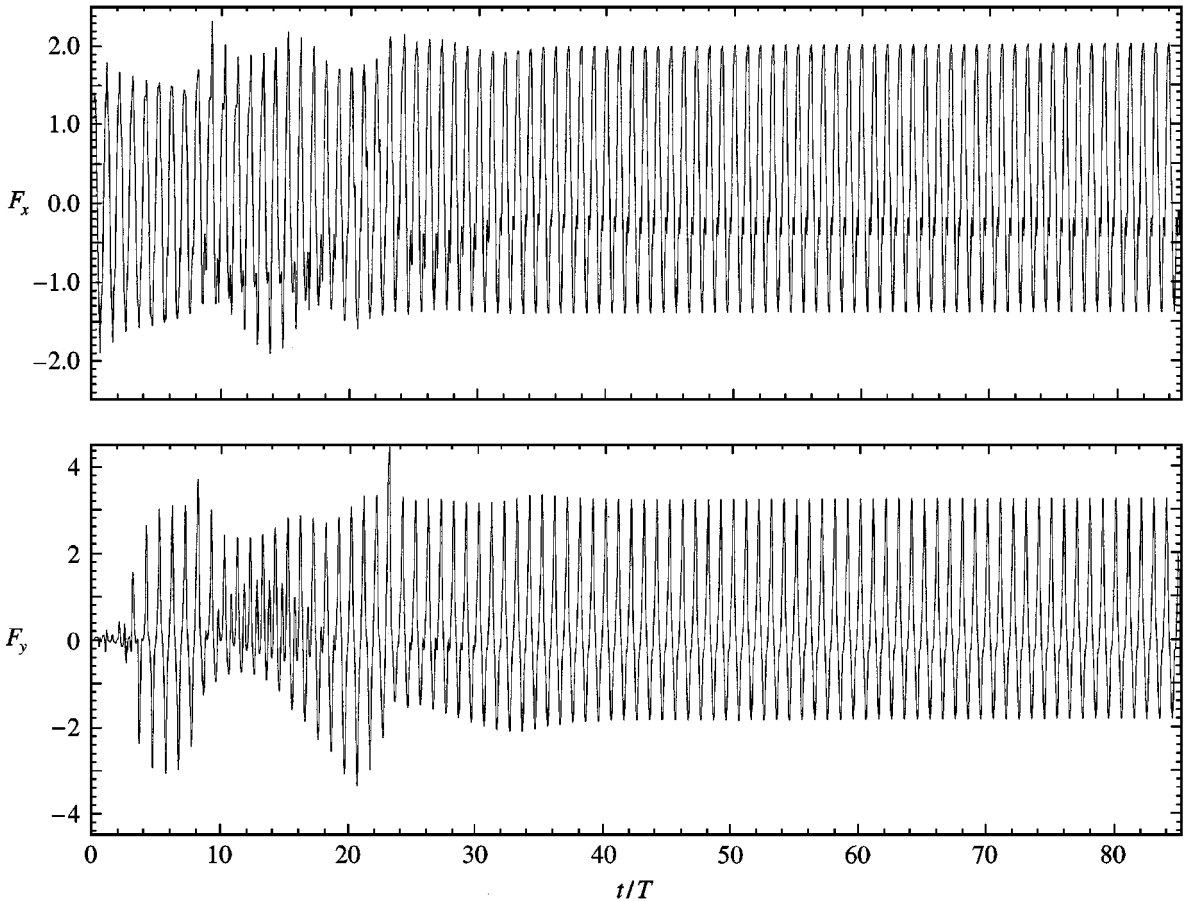

Figure 25. Time history of the hydrodynamic forces exerted on the cylinder for $f_f/f_n = 1$ and KC = 20.

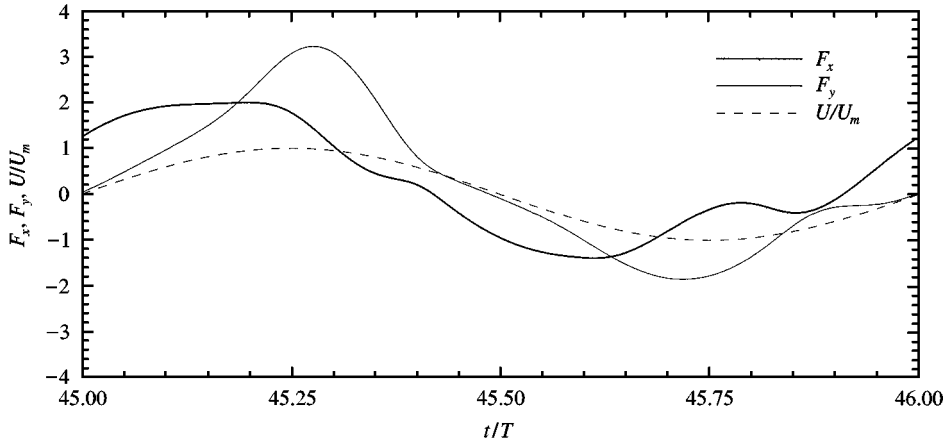

Figure 26. Traces of the hydrodynamic forces exerted on the cylinder and of the stream velocity over one oscillation cycle for $f_f/f_n = 1$ and KC = 20.

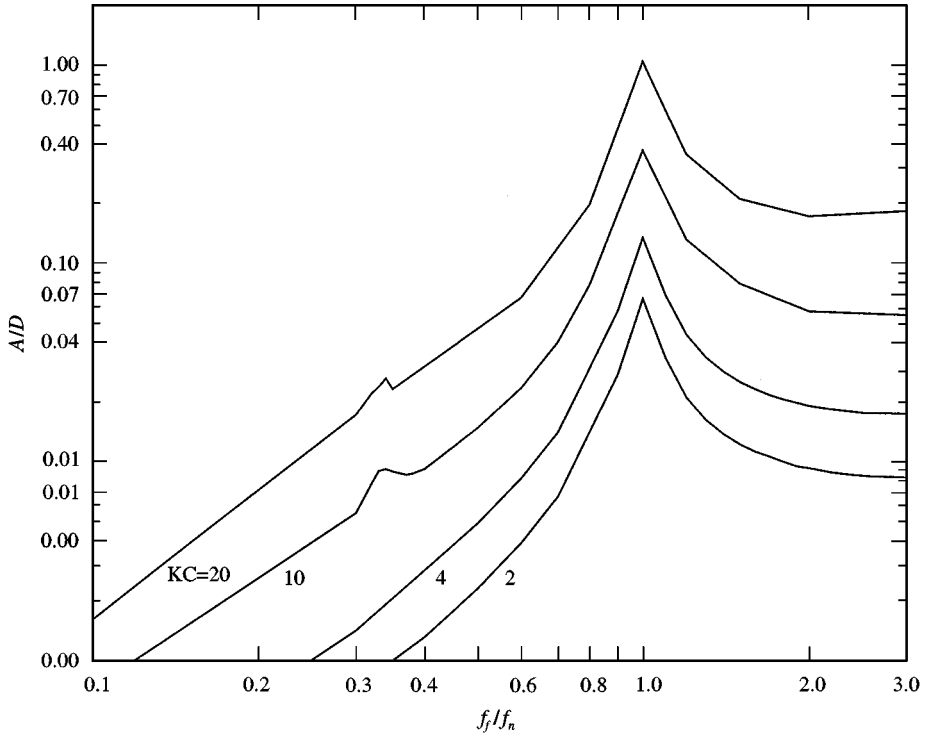

Figure 27. Oscillation amplitude at steady state as function of the frequency ratio; the cylinder mass was 0·01 kg, and the damping ratio 0·05.

the term $\rho A\dot{U}(i)$ was subtracted from $F_x^*(i)$. After back-substitution, the force traces derived from equation (23) were found to be in good agreement with those of the numerical simulation.

The values of the drag and added mass coefficients C_D and C_I for KC equal to 2, 4 and 10 are presented in Figures 28 and 29, throughout the range of f_r examined. Figure 28 indicates that there exists an abrupt decrease in C_D near resonance for all KC numbers. For a given frequency ratio, the C_D values for KC = 2 are almost the same as for KC = 4, except in the zone near resonance, where the C_D values for KC = 2 are lower. For KC = 10, the values of C_D are higher throughout the range of frequency ratios examined, except in the case when f_r lies around 0·33. Since the drag force determines the energy input on a flexible structure, it is evident that the higher C_D values with increasing KC in the zone near resonance are compatible to the response diagram of Figure 27. The relative velocity is not drastically different from the stream velocity for KC ranging between 2 and 10 as can be deduced from Figure 20, therefore, the drag term of the in-line force varies almost linearly with C_D. The values of C_I for KC equal to 2 and 4 are almost independent of the frequency ratio except in the resonance zone, where decreased values are observed. For KC = 10 the values of C_I are lower, except for $f_r = 1$, where a sudden increase is detectable. When KC equals 10 the decrease of C_1 for f_r around 0·33 is also observed.

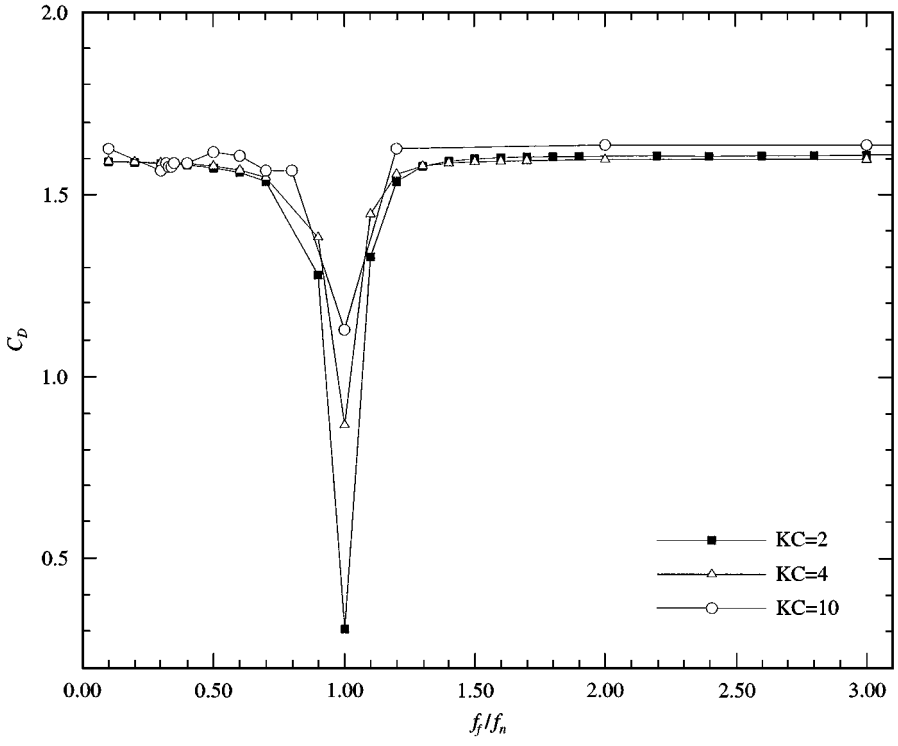

Figure 28. Drag coefficient as a function of frequency ratio, for three values of KC.

4. CONCLUSIONS

The finite element method was used for the numerical solution of planar oscillatory flow around an elastically mounted cylinder free to oscillate in the streamwise direction, at Re = 200 and KC ranging between 2 and 20. For each KC considered, computations were conducted for a wide range of frequency ratios, the frequency ratio being defined as the frequency of the oscillating stream to the natural frequency of the cylinder. For KC extending up to 4, the flow is symmetrical with respect to the wake centre-line and the in-line force is almost sinusoidal, giving rise to high amplitude cylinder response only at resonance. For KC equal to 10 and 20, the flow pattern produces an in-line force which contains components at the odd multiples of the flow oscillation frequency in addition to the fundamental. These higher components, especially that closest to the flow frequency, cause amplification of the cylinder response when their frequency is close to the natural frequency of the cylinder, apart from that occurring at resonance.

The large oscillation amplitude at resonance has a drastic effect on the flow pattern and on the hydrodynamic forces exerted on the cylinder, especially for KC equal to 10 and 20. When the cylinder oscillates, the effective Keulegan–Carpenter number is that based on the relative velocity of the fluid with respect to the moving cylinder. The modification of the effective Keulegan–Carpenter number due to the cylinder motion alters significantly the flow pattern around the oscillating cylinder, since the flow is very sensitive even to small variations of the Keulegan–Carpenter number in this low KC-β regime.

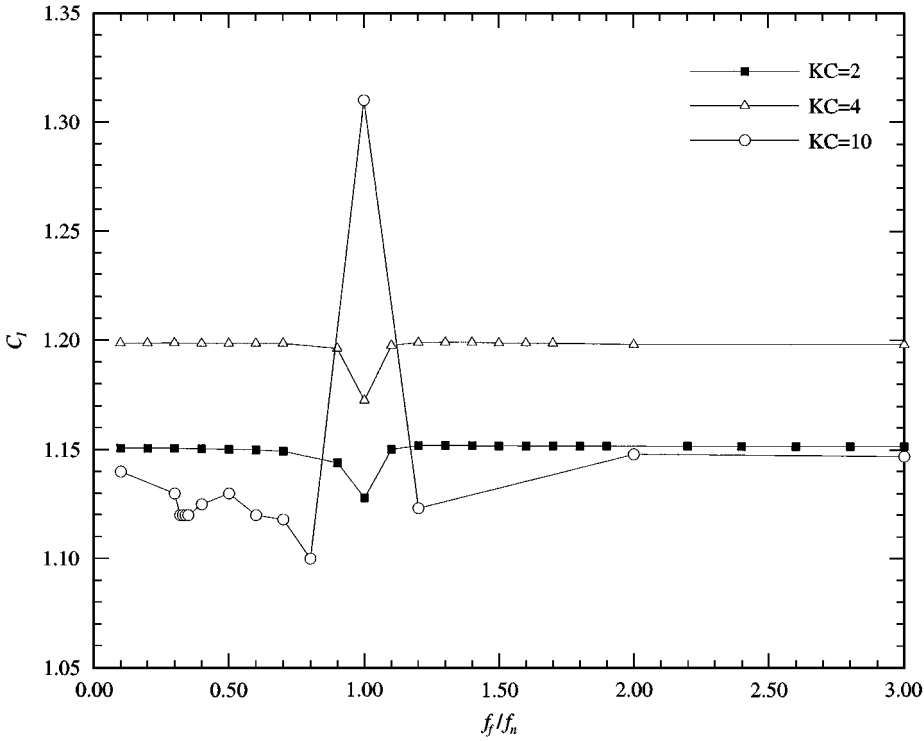

Figure 29. Added mass coefficient as a function of frequency ratio, for three values of KC.

The oscillation amplitude when the frequency ratio is maintained constant increases with the Keulegan–Carpenter number. The resolution of the in-line force revealed that the drag component was higher with increasing KC near resonance, although for constant KC the C_D values displayed a serious reduction when the frequency ratio was approaching 1. Since the drag force determines the energy input on a flexible structure, the higher drag values with increasing KC in the zone near resonance are compatible to the increased cylinder response.

ACKNOWLEDGEMENT

The present project was supported financially by the Science Programme of the European Community, Contract No SC1*-CT92-0812. G. Iliadis was subsidised by the Greek Foundation of National Awards (IKY).

References

Anagnostopoulos, P. 1989 Numerical solution for laminar two-dimensional flow about a fixed and transversely oscillating cylinder in a uniform stream. *Journal of Computational Physics* **85,** 434–456.

Anagnostopoulos, P. 1994 Numerical investigation of response and wake characteristics of a vortex-excited cylinder in a uniform stream. *Journal of Fluids and Structures* **8,** 367–390.

Anagnostopoulos, P., Iliadis G. & Ganoulis, J. 1995 Flow and response parameters of a circular cylinder vibrating in-line with the oscillating stream. In *Proceedings of the 6th International Conference on Flow-Induced Vibration* (ed. P. W. Bearman), pp. 167–179. London, U.K.

Anagnostopoulos, P., Iliadis, G. & Rasoul, J. 1993 Numerical solution of oscillatory flow around a circular cylinder at low Reynolds and Keulegan–Carpenter numbers. In *Proceedings of the Eight International Conference on Finite Elements in Fluids* (eds K. Morgan, E. Onate, J. Periaux, J. Peraire & O. C. Zienkiewicz), pp. 258–267. Barcelona, Spain.

Baba, N. & Miyata, H. 1987 Higher-order accurate difference solutions of vortex generation from a circular cylinder in an oscillatory flow. *Journal of Computational Physics* **69,** 363–396.

Bearman, P. W., Graham, J. M. R., Lin, X. W. & Mackwood, P. R. 1994 Modelling the cross-flow response of cylinders in oscillatory flow. In *Proceedings of the 7th International Conference on Behaviour of Offshore Structure* (*BOSS* '94), (ed. C. Chryssostomidis), Vol. 2, pp. 827–843. M.I.T. Boston, U.S.A.

Bearman, P. W., Graham, J. M. R., Naylor, P. & Obasaju, E. D. 1981 The role of vortices in oscillatory flow about bluff bodies. In *Proceedings of the International Symposium on Hydrodynamics in Ocean Engineering*, *The Norwegian Inst. of Technology* (ed. K. M. Gisvold), Vol. 1, pp. 621–635. Trondheim, Norway.

Bearman, P. W. & Hall, P. F. 1987 Dynamic response of circular cylinders in oscillatory flow and waves. In *Proceedings of the International Conference on Flow Induced Vibrations*, BHRA (ed. R. King), pp. 183–190. Bowness-on-Windermere, U.K.

Bearman, P. W., Lin, X. W. & Mackwood, P. R. 1992 Measurement and prediction of response of circular cylinders in oscillating flow. In *Proceedings of the 6th International Conference on Behaviour of Offshore Structures* (*BOSS* '92) (eds H. H. Patel & R. Gibbins), Vol. 1, pp. 297–307. London, U.K.

Bearman, P. W. & Mackwood, P. R. 1991 Non-linear vibration characteristics of a cylinder in an oscillating water flow. In *Proceedings of the IMechE International Conference on Flow Induced Vibrations* (ed. B. L. Clarkson), pp. 21–31. Brighton, U.K.

Blevins, R. D. 1977 *Flow-Induced vibration.* New York: Van Nostrand Reinhold.

Borgman, L. E. 1972 Statistical models for ocean waves and wave forces. *Advances in Hydroscience* **8,** 139–181.

Borthwick, A. G. L. & Herbert, D. M. 1990 Resonant and non-resonant behaviour of a flexibly mounted cylinder in waves. *Journal of Fluids and Structures* **4,** 495–518.

Graham, J. M. R. & Djahansouzi, B. 1989 Hydrodynamic damping of structural elements. In *Proceedings of the 8th International Conference on Offshore Mechanics and Arctic Engineering* (eds J. S. Chung, H. Maeda & T. Huang), Vol. 2, pp. 289–293. The Hague, The Netherlands.

Graham, J. M. R. & Djahansouzi, B. 1991 Computation of vortex shedding from rigid and compliant cylinders in waves. In *Proceedings of 1st International Offshore and Polar Engineering Conference* (eds J. S. Chung, M. Isaacson & H, Maeda), Vol. 3, pp. 504–508. Edinburgh, U. K.

Iliadis, G. & Anagnostopoulos, P. 1997*a* Viscous oscillatory flow around a circular cylinder at low Keulegan–Carpenter numbers and frequency parameters. *International Journal for Numerical Methods in Fluids*, **26**, 403–442.

Iliadis, G. & Anagnostopoulos, P. 1998*b* Numerical visualization of oscillatory flow around a circular cylinder at $\mathrm{Re} = 200$ and $\mathrm{KC} = 20$ – An aperiodic flow case. *Communications in Numerical Methods in Engineering*, **14**, 181–194.

Isaacson, M., Subbiah, K. & Baldwin, J. 1991 Force coefficient estimation from random wave data. In *Proceedings of the 1st International Offshore and Polar Engineering Conference* (eds J. S. Chang, I. Isaacson & H. Maeda), Vol. 3, pp. 149–157. Edinburgh, U. K.

Justesen, P. 1991 A numerical study of oscillating flow around a circular cylinder. *Journal of Fluid Mechanics* **222,** 157–196.

Lipsett, A. W. & Williamson, I. D. 1994 Response of a cylinder in oscillatory flow. *Journal of Fluids and Structures* **7,** 681–709.

McConnell, K. G. & Park, Y. S. 1982 The frequency components of fluid lift forces acting on a cylinder oscillating in still water. *Experimental Mechanics* **22,** 216–222.

Maull, D. E. & Kaye, D. 1988 Oscillations of a flexible cylinder in waves. In *Proceedings of the 5th International Conference on Behaviour of Offshore Structures* (*BOSS '88*) (eds T. Moan, N. Janbu & O. Faltinsen), Vol. 2, pp. 535–547. Trondheim, Norway.

Mittal, S. & Tezduyar, T. E. 1992 A finite element study of incompressible flows past oscillating cylinders and airfoils. *International Journal for Numerical Methods in Fluids* **15,** 1073–1118.

Morison, J. R., O'Brien, M. P., Johnson, J. W. & Schaaf, S. A. 1950 The force exerted by surface waves on piles. *Petroleum Transactions* **189,** 149–157.

Murashige, S., Hinatsu, M. & Kinoshita, T. 1989 Direct calculations of the Navier-Stokes equations for forces acting on a cylinder in oscillatory flow. In *Proceedings of the 8th International Conference on Offshore Mechanics and Arctic Engineering* (eds J. S. Chung, H. Maeda & T. Huang), Vol. 2, pp. 411–418. The Hague, The Netherlands.

Nomura, T. 1993 Finite element analysis of vortex-induced vibrations of bluff cylinders. *Journal of Wind Engineering and Industrial Aerodynamics* **46–47,** 587–594.

Nomura, T. & Hughes, T. J. R. 1992 An arbitrary Lagrangian–Eulerian finite element method for interaction of fluid and a rigid body. *Computer Methods in Applied Mechanics and Engineering* **95,** 115–138.

Sarpkaya, T. 1986 Forces on a circular cylinder in viscous oscillatory flow at low Keulegan–Carpenter numbers. *Journal of Fluid Mechanics* **165,** 61–71.

Skomedal, N. G., Vada, T. & Sortland, B. 1989 Viscous forces on one and two circular cylinders in planar oscillatory flow. *Applied Ocean Research* **11,** 114–134.

Smith, S. L. & Brebbia, C. A. 1975 Finite-element solution of Navier–Stokes equations for transient two-dimensional incompressible flow. *Journal of Computational Physics* **17,** 235–245.

Smith, S. L. & Brebbia, C. A. 1977 Improved stability techniques for the solution of Navier–Stokes equations. *Applied Mathematical Modelling* **1,** 226–234.

Smith, P. A. & Stansby, P. K. 1991 Viscous oscillatory flows around cylindrical bodies at low Keulegan–Carpenter numbers using the vortex method. *Journal of Fluids and Structures* **5,** 339–361.

Tatsuno, M. & Bearman, P. W. 1990 A visual study of the flow around an oscillating cylinder at low Keulegan–Carpenter number and low Stokes numbers. *Journal of Fluid Mechanics* **211,** 157–182.

Wang, X. & Dalton, C. 1991 Oscillating flow past a rigid circular cylinder: a finite difference calculation. *ASME Journal of Fluids Engineering* **113,** 377–383.

Wei, R., Sekine, A. & Shimura, M. 1995 Numerical analysis of 2D vortex-induced oscillations of a circular cylinder. *International Journal for Numerical Methods in Fluids* **21,** 993–1005.

Williamson, C. H. K. 1985 Sinusoidal flow relative to circular cylinders. *Journal of Fluid Mechanics* **155,** 141–174.

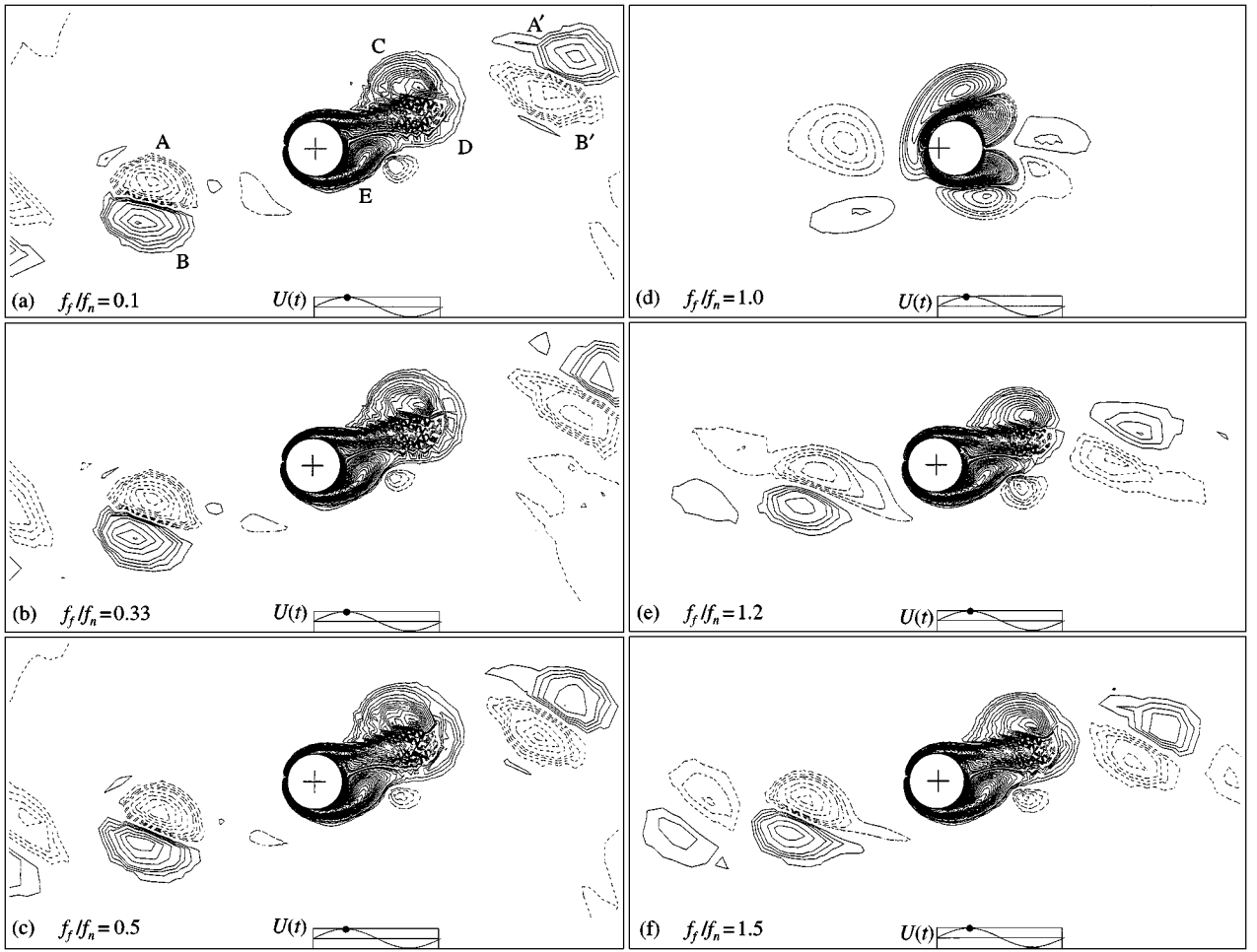

Figure 18. Equivorticity lines for various frequency ratios at phase angle $\phi = 93°$; KC = 10.

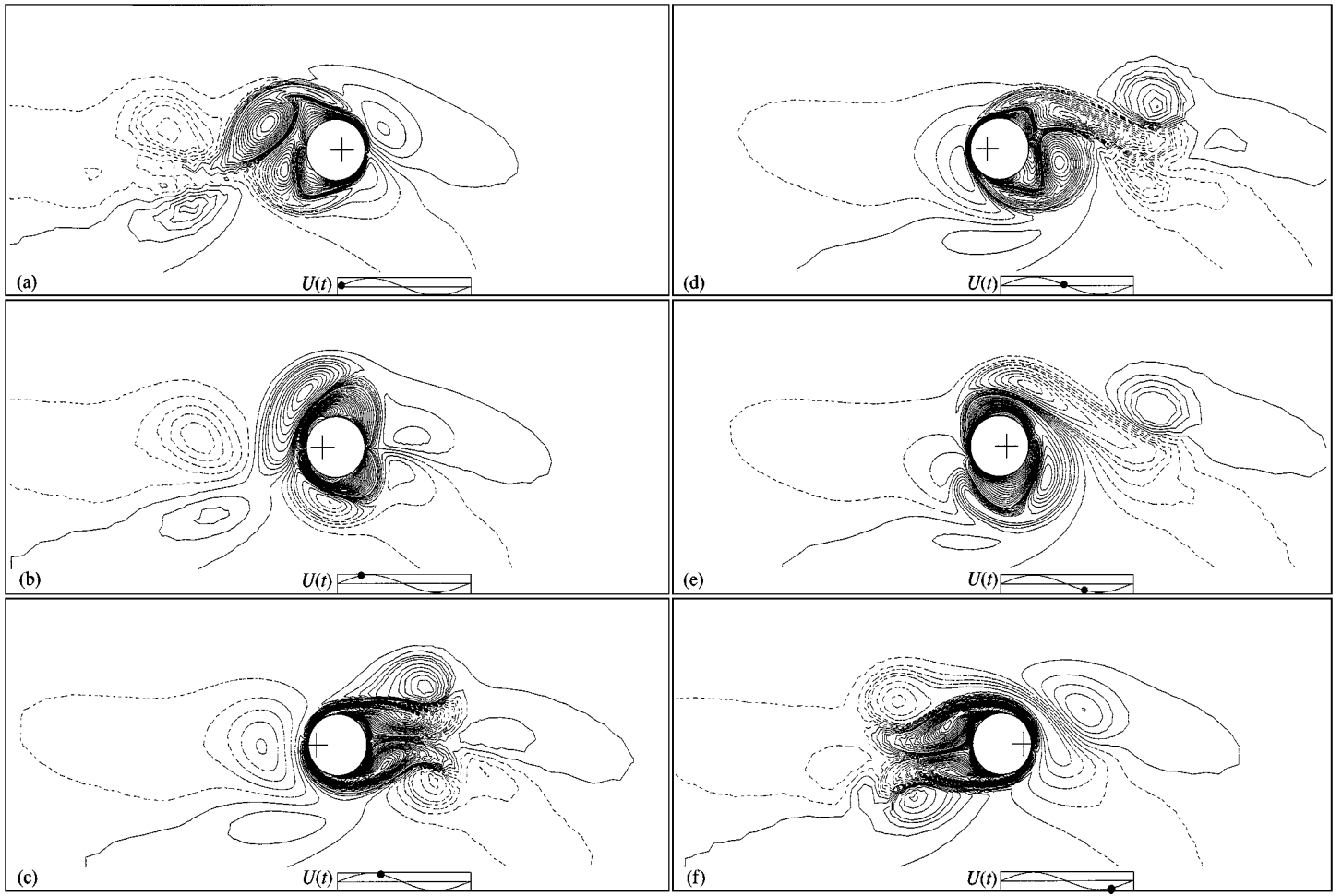

Figure 19. Equivorticity lines over one period for $f_f/f_n = 1$ and KC = 10.

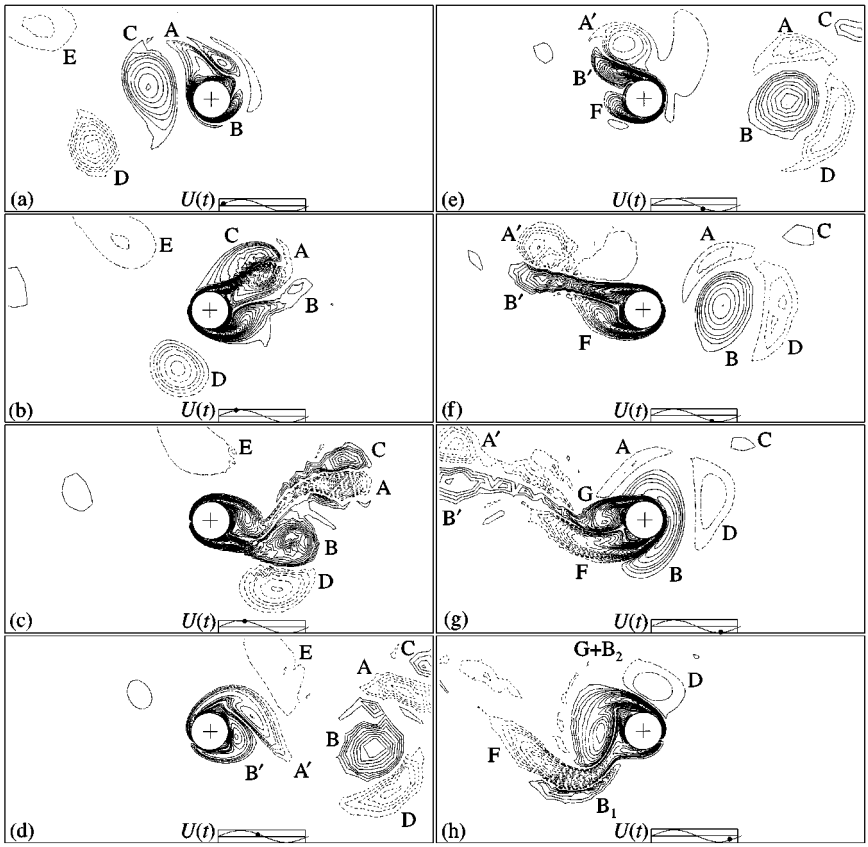

Figure 22. Equivorticity lines over one period for $f_f/f_n = 0{\cdot}33$ and KC = 20.

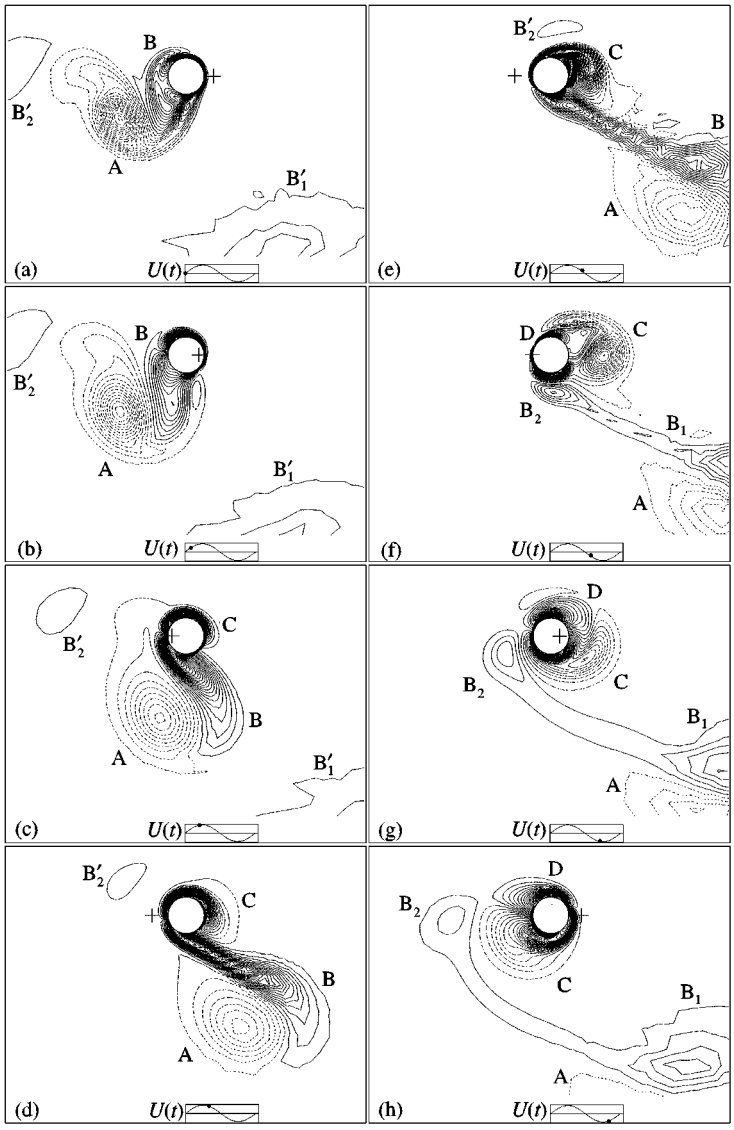

Figure 24. Equivorticity lines over one period for $f_f/f_n = 1$ and KC = 20.